

# **Numerical Studies on the Dynamics of Soft Matter Systems**

Thesis submitted for the degree of

Doctor of Philosophy (Sc.)

in

Physics (Theoretical)

by

**Suman Dutta**

Department of Physics

University of Calcutta

2018

*This page belongs to  
My Mother  
who is Right-Hemiplegic*

*This page belongs to  
My Father  
who is Left-Hemiplegic*

*Talent hits a target no one else can hit. Genius hits a target no one else can see.*

– Arthur Schopenhauer

# Prologue

*This dissertation is submitted for the degree of Doctor of Philosophy at the University of Calcutta. The research described herein was conducted under the supervision of Prof. Dr. Jaydeb Chakrabarti in the Department of Chemical, Biological and Macro-Molecular Sciences, S. N. Bose National Centre for Basic Sciences, between August, 2012 and January, 2018.*

*The outcome of our research have been published and communicated as -*

- Suman Dutta and J. Chakrabarti, *Anomalous dynamical responses in a driven system*, EPL (Europhys. Lett.), **116**, 38001 (2016)
- Suman Dutta, *Microscopic insights into dynamical heterogeneity in a lane forming system*, arXiv:1711.09779 (Communicated, 2017)
- Suman Dutta and J. Chakrabarti, *Transient dynamical responses of a charged binary colloid in an electric field* (Communicated, 2018)
- Suman Dutta and J. Chakrabarti (In preparation)

*Prof. Dr. C. Dasgupta(IISc), Dr. S. Karmakar(TIFR-H), Dr. T. Das (NIST) and Dr. S. Chatterjee(SNBNCBS) are acknowledged for discussions. Prof. Dr. S. Sastry (JNCASR), Dr. R. De(IISER-K) and Dr. P. Chaudhuri(IMSC) are also acknowledged for offering opportunities to present the research that is a part of this thesis.*

*Prof. Dr. M. Acharyya (Presidency University), Prof. Dr. R. Biswas and Dr. S. Chatterjee(SNBNCBS) are acknowledged for their comments, constructive criticisms and fruitful suggestions as members of Thesis committee with Prof. Chakrabarti.*

*A special mention goes to the present (Sutapa, Piya, Arunabha, Edwin and Darshan ) and past members ( Dr. M. Ghosh, Dr. A. Das, Dr. S. Sikdar, P. Saha, A. Bhowmick) of my group for every possible reasons. I also thank the entire SNBNCBS fraternity for the facilities, fellowship and making my life beautiful during the period of stay as a Post. B.Sc Integrated Ph.D Research (PBIR) fellow.*

# Abstract

In this thesis, attempts have been made to explore the interplay between dynamics and structural changes in a simple system of a binary mixture of oppositely charged colloidal particles driven by a constant electric field using Brownian Dynamics Simulations. This is widely regarded as a generic model of pattern forming non-equilibrium systems. The system is known to form microscopic lanes of like charges along the field. The scenario resembles laning in a host of systems found in nature. We observe crossover in dynamics: from an initial fast relaxation in the homogeneous state to a slowed-down lane state. There is an intermediate pre-lane state with anomalous dynamical responses, namely, a non-Fickian exponential tail in self-van Hove functions and a stretched exponential relaxation in both self-overlap functions and distinct van Hove functions. The probability distribution of particle diffusion broadens due to the coexistence of competing timescales of relaxation in the pre-lane state.

Furthermore, we investigate the growth in structural heterogeneity as electric field is turned on equilibrium system in transient condition. The aging persists till the system reaches steady states. We show that the lifetime of anomaly in dynamical responses depends upon the time of observations after the field is turned on. The formation of heterogeneous structures shows signature of aging. The aging is not present when the steady states relax back to equilibrium in absence of the field. There are two structural length-scales in the system characterizing correlation in a given species and that between cross-species, grows at distinct rates, though both follow algebraic growth. The spatial length-scale of dynamic heterogeneity is identified in terms of length-scale of structural correlation between the particles of different mobilities. These length-scales are correlated in transient conditions and become independent in steady states. The thesis also discusses the possible implications of our research.

# Contents

<b>Prologue</b>	<b>i</b>
<b>Abstract</b>	<b>ii</b>
<b>1 Introduction</b>	<b>1</b>
<b>2 Methods</b>	<b>8</b>
2.1 Model . . . . .	8
2.2 Algorithm . . . . .	9
2.3 Data Analysis . . . . .	9
2.3.1 Structural Quantities . . . . .	10
2.3.2 Dynamical Quantities . . . . .	11
<b>3 Steady State Structures</b>	<b>12</b>
3.1 Lane order parameter . . . . .	12
3.2 Density Profiles . . . . .	13
3.3 Pair Correlation Function . . . . .	14
3.4 Cluster-size distribution . . . . .	16
3.5 Discussion . . . . .	17
3.6 Conclusion . . . . .	18
<b>4 Dynamical Response in Steady States</b>	<b>19</b>
4.1 Self van Hove functions . . . . .	19
4.2 Particle resolved picture . . . . .	22
4.3 Distinct van Hove functions . . . . .	23
4.4 Discussion . . . . .	26
4.5 Conclusions . . . . .	26

<b>5</b>	<b>Structural Relaxation in Steady States</b>	<b>27</b>
5.1	Overlap Function . . . . .	27
5.2	Relaxation of the partial structures . . . . .	29
5.3	Discussion . . . . .	32
5.4	Conclusion . . . . .	33
<b>6</b>	<b>Transient Response</b>	<b>34</b>
6.1	Growth of Heterogeneous Structures . . . . .	34
6.2	Transient Dynamical Response . . . . .	36
6.3	Aging in transient state: . . . . .	37
6.4	Relaxation of Heterogeneous Structures . . . . .	40
6.5	Discussion . . . . .	41
6.6	Conclusion . . . . .	41
<b>7</b>	<b>Dynamic Length-scales</b>	<b>43</b>
7.1	Length-scale of Structural Correlations . . . . .	43
7.2	Dynamic Length-scales . . . . .	46
7.3	Discussion . . . . .	48
7.4	Conclusion . . . . .	49
	<b>Epilogue</b>	<b>50</b>

# Chapter 1

## Introduction

Soft Materials are complex systems that are susceptible to external perturbations [1]. The size of the particles in these systems falls between the microscopic and the macroscopic regimes [2]: They are big enough to behave like classical particles but small enough for thermal motion [3,4]. These materials show fascinating phenomena, ranging from emergence of patterns to self-assembly, relevant in different areas of interdisciplinary sciences bridging physics, chemistry, biology and engineering [1–7]. These phenomena are often described in terms of continuum phenomenological models [8,9] where microscopic description on particle scales is largely lacking [7]. The microscopic description of these phenomena are not only pedagogically challenging but also would be immensely important in technological applications [10].

Colloids are ideal model system for understanding equilibrium and non-equilibrium phenomena found in soft matter systems [5–7]. Due to their large size, their motion is slow that can be tracked in experiments [2–7]. Laning is a typical example of pattern formation in systems realized in a host of systems, like army ants [29], pedestrian movements [30], granular media [31], dusty plasma [32], dipolar microswimmers [33] out of equilibrium conditions [4–6, 11–33]. Colloids also show laning: Applying a constant electric field on a system of binary charged colloids, the system crosses over from a homogeneous mixture to a state with lanes of likely charged particles elongated parallel to the field [5, 6, 11–28]. The lane formation has been affirmed in experiments [16, 20] where binary mixture of charged colloidal particles in a capillary are subject to electric field. The oppositely charges are fluorescently labelled with die in order to tag the color-coded particles. The Debye-Hückel screening length [34] of the particles can be manipulated in these experiments [5–7]. The particles are tracked in real time in real space using confocal microscopy [16, 20]. The confocal images are analyzed to track the particle trajectories. From the initial mixed state, particles form lanes along the field within a very short

time [20]. The projection of the lanes in the transverse plane show domains of like charges. These domains proliferate along the direction of the field. The formation of the lanes are accompanied by enhanced diffusion. The diffusion decreases significantly for high field indicating slowing down [20]. These experiments also affirm the presence of slow and fast particles in the system, suggesting dynamic heterogeneity in steady states [20]. The particles in the lanes are different from the particles not in the lanes. On withdrawal of the field, the system relaxes back to the initial state again, suggesting an absence of hysteresis [20].

There are theoretical studies, including computer simulations on lane formation [11–15, 17, 21–28], in both two [11–15, 21, 22, 24, 25] and three dimensions [17, 23, 26–28]. There is a prediction of dynamic instability of the homogeneous state in the form of a re-entrant effect in lane formation: Lane formation occurs only within a finite density window for a particular field strength. The critical field strength for lane formation also depend upon the density of particles. This has been supported by analytical results using the phenomenological Dynamical Density Functional Theory (DDFT) [12, 13]. The phase diagram of the laning transition has been obtained for the model with and without hydrodynamic interactions (HI) [7, 17]. The experiments are in good agreement with the results obtained previously in different studies without HI, suggesting that HI does not contribute much to explain lane formation in driven colloids [20]. The particle correlations grow algebraically with field strength in two dimensions [22, 25]. The growth in particle correlation has been observed in both theoretical and analytical results. The correlation decays exponentially in the transverse plane and algebraically along the field [25].

In this thesis, we project lane forming system as a model system of pattern forming non-equilibrium systems. Our objectives are as follows:

- Microscopic structures on particle scale in steady states away from equilibrium.
- Dynamic response in non-equilibrium steady states.
- Structural relaxation in steady states.
- Transient responses when a structurally homogeneous equilibrium state approaches non-equilibrium steady states with structural heterogeneity.
- Growth of correlations during formation of heterogeneous structures.

We simulate a three-dimensional system of colloidal particles of same size and opposite charges with equal proportion in a highly viscous solvent media. The particles interact pairwise: The opposite charges attract, while the like charges repel each other via the Derjaguin-Landau-Verwey-Overbeek (DLVO) [35, 36] potential. The thermal bath is kept at a constant temperature which is the source of fluctuation in the system. Due to the high viscosity of the medium, the motion of the particles is over-damped. We integrate the equation of motion of individual particles to generate the particle trajectories following Ref. [37]. We initialize the system with random configurations. We let this system to equilibrate without the external electric field. Then a constant unidirectional electric field is turned on to drive the system away from its equilibrium to reach non-equilibrium steady states with patterns of like charges parallel to the field as lanes. We also study the cases where these steady state patterns are relaxed on withdrawal of the field so that the system reaches the equilibrium state again.

We analyze structures and dynamics in the steady states and in transient conditions. The microscopic structures have been monitored via the lane order parameter [17]. These structures are realized via density profiles [38]. The ordering in the structures are captured by the pair correlation functions (PCF) [38] which is the probability of separation between a pair of particles. We study dynamics using the van Hove functions (vHf) [39]. The vHf consists of two parts: self and distinct [38, 39]. Self-van Hove functions (self-vHf) is the probability of particle displacement in a given time interval [38, 39]. The relaxation of the structures is monitored via the distinct van-Hove function (distinct-vHf) which is the probability of pair separation in a given time interval, captures the relaxation of structures due to diffusion [38, 39]. Self-Overlap function provides the fraction of particles having displacement within a critical limit in a given time interval [40, 41]. Dynamic susceptibility captures the dynamic fluctuation in the self-Overlaps show the structural response [40, 41]. In all the cases, we average the dynamical and structural quantities over the Brownian trajectories generated with different initial configurations. This is to ensure that the particles explore the full phase space and averaged over noise [42, 43].

*Microscopic Structures:* The density profiles show changes in structures in the plane transverse to the field. For sufficiently high value of the field, in the transverse plane shows small domains of like charges. Along the field, these domains are elongated. They proliferate as lanes for the very high field while the patterns in the transverse plane are similar to network like structures. The PCFs capture the order in these structures: A sharp peak at a particle separation between the opposite charges in PCFs in the equilibrium suggests that the equilibrium state is dominated by Coulomb attraction between the opposite pairs. A broad peak is seen

in PCF between the like charges at more than two particle separation indicates that particles only sit opposite-pairwise in this state. For finite values of the field, the sharp peak in the PCF between opposite charges decays and the broad peak in PCF between the like charges increases. Also, in all these cases, higher coordination shells are seen in PCFs among both the like and cross charges when the domains of like charges are present. The PCFs also show asymmetry along the field with algebraic decay opposite to the field direction. The co-operativity of the like charges in lanes is quantified in terms of clusters of particles with similar charges residing within a critical distance. In the equilibrium, there are many isolated clusters. In contrast, in the lane state, there are fewer but bigger clusters as lanes. In the steady state with the intermediate field, there are many clusters with different sizes which we define as the *pre-lane* state. Hence, the spread in the cluster size distribution has a maximum in the *pre-lane* state. We study dynamics in these three typical situations.

*Dynamic response:* In absence of electric field, the self-vHf is a symmetric Gaussian as in normal liquids. As soon as the field is turned on, the self-vHf along the field is Gaussian but the peak starts shifting. The drift in the peak position depends on the strength of the field. The width in the distribution becomes asymmetric with respect to the field. The self-vHf develops an exponential tail in the *pre-lane* state and becomes double Gaussian in the lane state. However, opposite to the field, the self-vHf remains Gaussian. In the transverse plane, the dynamics is similar to that along the field.

The exponential tail has been described earlier in terms of heterogeneity in dynamics in a system [44]. The individual particle motion is tracked. The particles are randomly picked from different structural regions of the system. The probability distribution of particle displacement shows that particle motion is diffusive. The second moment in the probability distribution of particle displacement shows different slopes in different time, suggesting heterogeneity in diffusion. The diffusivities are collated to compute the diffusion spectrum. The diffusion spectrum has a peaked form in the homogeneous state. This broadens in the *pre-lane* state. In the lane state, there is a re-entry of the peaked form of the diffusion spectrum, albeit with a tail towards higher diffusion. The primary peak in the spectrum shifts to the lower diffusion values indicating a slowing down in the transverse plane. The heterogeneity in the diffusion is maximum in the *pre-lane* state.

The distinct-vHf equals to the PCFs when the time interval is zero. The distinct-vHfs between the like charges in the Fourier space has a peak while that between the opposite charges has a dip. The decay of the peak and the dip with time gives the structural relaxation. The structural relaxation between the like charges is a direct measure of the relaxation of like

charges that mostly resides in the lanes, while that between the opposite charges quantifies the relaxation of the lane interfaces since the opposite charges comes only in contact at the lane interfaces. The distinct-vHfs show exponential decay except between the opposite charges in the *pre-lane* state. In this case, the relaxation follows slow stretched exponential dependence. The slow relaxation is phenomenologically interpreted via the Vineyard's approximation which connects the particle structure to relaxation due to diffusion. When the change in structure is within first order in the lane order parameter, the slow relaxation can be accounted for by the presence of exponential tail.

*Structural relaxation:* The overlap function has been previously tested with success in glass-forming liquids in exploring the slowing down [40, 41]. The overlap function captures the slowing down in the system undergoes crossover. In both the homogeneous and the lane state, the overlap function shows algebraic decay as in complex liquids [45]. In the *pre-lane* state, the overlap function show slow stretched exponential dependence. The dynamic susceptibility captures the dynamic fluctuation in the overlap function, show heterogeneity in terms of distinct peaks in the lane state due to distinct response in fast and slow particles. There is simultaneous presence of slow and fast particle in the system. The slow and fast relaxing particles are identified from the distribution of particle displacements in a given time window. The partial distinct-vHfs are constructed between these slow and fast relaxing particles within the particular time-window. The relaxation of these partial structures follows exponential decay. However, the decay rates are different. The heterogeneity in relaxation times is maximum in the *pre-lane* state.

*Transient Response:* We, further, study the evolution of the system after application of electric field onto the system in equilibrium. When a system is disturbed from its equilibrium, the physical quantities evolve with time to reach a new state. The new state may be an equilibrium state or a steady state far from equilibrium [8]. The time dependence of different dynamical quantities during the evolution describes the transient response. Although near-equilibrium treatments have been applied successfully to understand transition between equilibrium states [8], microscopic description of transient response while approaching steady states is still lacking [3,4]. This is relevant in understanding the kinetics of pattern formation [9] in non-equilibrium steady states observed in a host of systems [2].

On application of the field, the homogeneous equilibrium state starts evolving and reaches non-equilibrium steady states. The lane order parameter increases with the time of observations after application of the field. For different values of the field strength, the system reaches steady states in different times. The self-vHfs are analyzed in transient conditions. For small field,

in the homogeneous state, the self-vHfs are Gaussian for all times of observations. As the system is driven to the pre-lane state, the self-vHfs develop the exponential tail much before the steady state is reached. Similarly, the self-vHf becomes double Gaussian before the laning is complete for larger field strength. Single particle diffusion coefficient also depend on the times of observation. The diffusivities decrease as the system ages till the system approaches the steady states. The aging is absent when the steady states approach the equilibrium states on withdrawal of the field, suggesting the dynamical routes of growth and relaxation of the heterogeneous structures are different.

*Growth of Correlation:* The development in structural correlation has been probed via the time-dependent PCFs. The development in structural correlation length follows algebraic dependence on the age of the system. This growth takes place till the system reaches the steady states. Once it reaches the steady states, the correlation between opposite charges decays slowly suggesting coarsening of the lanes. The dynamic heterogeneity suggested by the distribution of diffusion coefficients indicates the presence of slow and fast particles simultaneously in the system. The length-scales between slow particles in both the species, show similar behavior. These length scales are correlated during the transient conditions, but they become independent in steady states.

In brief, we observe in-homogeneous structures in a binary mixture of oppositely charged colloid due to competing interaction which could be tuned by the applied field. We identify field driven dynamical state having anomalous dynamical responses with exponential tail in self-vHf and stretched exponential relaxation in distinct-vHf. The particle diffusion here is having a distribution, instead of a single diffusion coefficient. In transient conditions, the anomaly in dynamical response depends on the age of the system once field is switched on. The aging persists till the steady states are reached. Our results show the existence of multiple growing length-scales in the system. We show that these length-scales are correlated during the formation of the structures and are independent in steady states.

These results are not only relevant in the context of lane formation but also would be pertinent in a host of soft matter systems that show the emergence of structure due to competing interaction under drive. This situation is often encountered in areas of rheology, micro-fluidics and bio-molecular systems [10]. Also, it would be interesting to check whether the dynamical response affect the visco-elastic and dielectric response of the system, not only in the present scenario but also in cases where similar charged or magnetic dipolar colloids are subject to oscillatory field, or confinement or both [63,64], in steady states, even in transient conditions.

The organization of the rest of this thesis is as follows: We first introduce the model and a

brief of methods in the following Chapter 2. Then we discuss our results of structural quantities in the steady states in Chapter 3. This is followed by our analysis of dynamical response in steady states in Chapter 4. In Chapter 5, the heterogeneity in steady state structural response has been discussed. Chapter 6 contains transient response where we discuss both, growth of heterogeneous structure and relaxation from heterogeneous structures. Chapter 7 lists heterogeneous correlation between dynamic length-scales in transient conditions.

# Chapter 2

## Methods

In this chapter, we briefly describe the model system (Sec. 2.1). This is followed by algorithm we use in the simulations (Sec. 2.2). The final part (Sec. 2.3) consists of a discussions on the dynamical and structural quantities we compute in different conditions.

### 2.1 Model

Our simulated system consists of a binary mixture of equal number of positively ( $N_+$ ) and negatively ( $N_-$ ) charged colloidal particles of diameter  $\sigma$  with ( $N_+=N_-$ ) in a solvent of viscosity  $\eta$  in a cubic box of length  $L$  at temperature  $T$  with the periodic boundary conditions. The hydrodynamic interaction has not been considered here.

The pair interaction between particles at positions  $\vec{R}_i$  and  $\vec{R}_j$  and separation  $r_{ij} = |\vec{R}_i - \vec{R}_j|$  is given by [17]

$$V(r_{ij}) = V_{SC}(r_{ij}) + V_{Repulsion}(r_{ij}). \quad (2.1)$$

Here,  $V_{SC}(r_{ij})$  has DLVO form [35, 36]:

$$V_{SC}(r_{ij}) = V_0 [q_i q_j / (1 + \frac{\kappa\sigma}{2})^2] [\exp(-\kappa\sigma((r_{ij}/\sigma) - 1)) / (r_{ij}/\sigma)]. \quad (2.2)$$

$V_{Repulsion}(r_{ij})$  has Weeks-Chandler-Anderson (WCA) form [46]:

$$V_{Repulsion}(r_{ij}) = \begin{cases} \varepsilon [(\sigma/r_{ij})^{12} - (\sigma/r_{ij})^6] + \frac{1}{4}, & \text{if } r_{ij} < 2^{1/6}\sigma. \\ 0, & \text{otherwise} \end{cases} \quad (2.3)$$

Here  $q_i (=q$  for all  $i$ ) is the charge of the  $i$ th particle,  $\kappa$  the inverse screening length,  $V_0$  the interaction strength parameter and  $\varepsilon = 4|q|^2 V_0 (1 + \kappa\sigma/2)^2$  [17].

We choose the parameters used in Ref. [17]. We take equi-molar binary mixture of particles with diameter  $\sigma (= 1\mu m)$  and charge  $\pm q$  in a viscous medium with viscosity  $\eta (= 1cP)$  in a cubic box of length  $L$  at temperature  $T (= 298K)$ . The screening length of the particle interaction has been fixed at  $\kappa\sigma = 5.0$  and  $V_0^* = |q|^2 V_0/k_B T = 50.0$ . We take  $\tau_\beta (= \sigma^2/D_0)$  as time unit,  $\sigma$  the length unit and  $k_B T$  the energy unit. Here,  $D_0 (= k_B T/3\pi\eta\sigma, k_B$  the Boltzmann constant) the Einstein-Stokes Diffusion coefficient.

The steady state data analysis is based on a system with  $N = 2000$  in a cubic box of length  $L = 21.599\sigma$ . Since averaging in transient conditions can be done only over trajectories, a bigger system is required for better statistics. In the transient condition, we consider a bigger system with  $N = 10000$  in a box with  $L = 36.827$  with same volume fraction and other parameters remain same.

## 2.2 Algorithm

The BD simulations [18] are carried out using the Langevin's equation in over-damped limit [37]:

$$\Gamma \frac{d}{dt} \vec{R}_i = qf_0 \hat{Z}_i + \vec{\nabla}_i \sum_{j=1}^N V(r_{ij}) + \vec{F}_i(t) \quad (2.4)$$

Eqn. (2.4) could be discretized as [17,37]-

$$\vec{R}_i(t + \Delta t) = \vec{R}_i(t) + \vec{F}_i(\Delta t) + \vec{\nabla}_i \sum_{j=1}^N V(r_{ij})\Delta t + qf_0 \hat{Z}_i \Delta t \quad (2.5)$$

Here,  $\Gamma (= 3\pi\sigma\eta)$  is the viscous damping and  $\vec{F}_i(t)$  the fluctuating force with variance  $\langle F_i^\alpha(t) F_j^\beta(t') \rangle = 2D_0 \delta_{\alpha\beta} \delta_{ij} \delta(t - t')$  where  $\alpha, \beta$  denote the cartesian components and  $D_0$  the Einstein-Stokes Diffusion coefficient with  $\Gamma D_0 = k_B T, k_B$  the Boltzmann constant. We take  $\tau_\beta = (\sigma^2/D_0)$  as unit time,  $d$  the length unit and  $k_B T$  the energy unit. The integration time step for Eq.(2.4)  $\Delta t = 0.00005$ .

## 2.3 Data Analysis

The data analysis has been performed for the structural and dynamic quantities in both steady states and transient conditions. The system is first initialized with random configurations and equilibrated with  $f = 0$ . We wait for  $100\tau_\beta$  and then, the field is turned on with non-zero  $f (= |q| f_0 \sigma / k_B T)$  so that the system reaches a steady state. The steady state statistics are gathered for  $50\tau_\beta$ . Finally the steady states are relaxed on withdrawal of the field ( $f = 0$ ) to

reach the equilibrium. Different such cases are studied for different values of  $f$ . The steady state statistics are averaged over configurations and  $N_T (= 20)$  Brownian trajectories. In transient conditions, we only average over the BD trajectories. The dynamical and structural quantities we compute are as follows:

### 2.3.1 Structural Quantities

#### (a) Lane Order Parameter

The tendency in laning is captured via the lane order parameter defined in [17],

$$\Phi = \langle \frac{1}{N} \sum_{i=1}^N \phi_i \rangle \quad (2.6)$$

is assigned to every particle with  $\phi_i = \frac{[n_l - n_o]^2}{[n_l + n_o]^2}$ . Here,  $n_l$  and  $n_o$  are the numbers of like-charged particles and oppositely charged particles, respectively, whose projections of distance onto the plane perpendicular to the field are smaller than a cutoff length scale  $z_c (= 0.75\sigma)$  and ' $\langle \rangle$ ' signifies averages over both the initial conditions and Brownian trajectories.

(b) *Single particle density*: Structural patterns are visualized via the single particle density [38, 42]. This is defined as the probability of finding a particle at  $\vec{r}$  given by [38]

$$\rho(\vec{r}) = (1/N) \langle \sum_{i=1}^N \delta(\vec{r} - \vec{R}_i) \rangle \quad (2.7)$$

Here  $\vec{R}_i$  is the position vector of  $i$ th particle.

(c) *Pair Correlation Functions (PCF)*: The steady state structural correlations are given by pair correlation functions (PCF) [38, 42] which are probability distributions of particle separation at  $\vec{r}$  at a given time. This is given by-

$$g(\vec{r}) = (1/N^2) \langle \sum_{i=1}^N \sum_{j \neq i} \delta(\vec{r} + (\vec{R}_j - \vec{R}_i)) \rangle \quad (2.8)$$

(d) *Cluster-size Distribution*: Identification of clusters use of a clustering algorithm in Ref. [42]. This is based on nearest-neighbor distance criterion in Ref. [47]. First a random particle  $i$  is picked. All other particles  $j$  that satisfy

$$r_{ij} < r_{cl} \quad (2.9)$$

where  $r_{cl}$  is a critical separation between two such particles, are defined to be in the same cluster as  $i$ . Each such particle  $j$  is added to the cluster, and is subsequently used in the same

way as  $i$ , to identify further members. The process goes till it finds no particles within  $r_{cl}$  for each of the particles contained in the cluster. Probability of having a cluster with size  $s$  in a system is given by  $P_{cluster}(s)$ . We use  $r_{cl} = 1.4\sigma$  for our calculation as suggested by Ref. [48]

### 2.3.2 Dynamical Quantities

(a) *van-Hove Function(vHf)*: This is defined as the probability of finding a particle at position  $r$  at time  $t$ , given that there was a particle at the origin at time  $t = 0$ , given by [38, 39] -

$$G(\vec{r}, t) = (1/N) \left\langle \sum_{i=1}^N \sum_{j=1}^N (\delta(\vec{r} + \vec{R}_j(0) - \vec{R}_i(t))) \right\rangle \quad (2.10)$$

It consists of two parts [38]:

(1) The self-vHfs: The probability distribution of displacements( $\vec{r}$ ) of individual particles in a given time interval  $t$  is given by [38, 39]

$$G_S(\vec{r}, t) = (1/N) \left\langle \sum_{i=1}^N \delta(\vec{r} + \vec{R}_i(0) - \vec{R}_i(t)) \right\rangle \quad (2.11)$$

(2) The distinct-vHfs: Probability distribution of particle separations ( $\vec{r}$ ) between a pair of particles over a time interval,  $t$  is given by [38, 39]

$$G_D(\vec{r}, t) = (1/N^2) \left\langle \sum_{i=1}^N \sum_{j \neq i}^N (\delta(\vec{r} + \vec{R}_j(0) - \vec{R}_i(t))) \right\rangle \quad (2.12)$$

(b) *Overlap Function*: Structural relaxation is generally interpreted via the evolution of self Overlaps [40, 41], given by given by

$$Q(t) \sim \frac{1}{N} \sum_{i=1}^N \psi(|\vec{R}_i(0) - \vec{R}_i(t)|) \quad (2.13)$$

Here,

$$\psi(r) = \begin{cases} 1, & \text{if } r \leq 0.3\sigma \\ 0, & \text{elsewhere} \end{cases} \quad (2.14)$$

(c) *Dynamical Susceptibility*:

The dynamical susceptibility is given in terms of the dynamic fluctuations in  $Q(t)$  [40, 41],

$$\chi_4(t) = \langle Q^2(t) \rangle - \langle Q(t) \rangle^2. \quad (2.15)$$

# Chapter 3

## Steady State Structures

Here we report the structural features in steady states [23] The details of the model system has been discussed in Sec. 2.1. We start with the equilibrium state and apply electric field along  $z$  direction. We describe structural features in the steady states in terms of lane order parameter (Sec 3.1), density profiles (Sec 3.2), PCF (Sec 3.3)and cluster size distribution(Sec 3.4). We discuss our results in Sec. 3.5 and we conclude in Sec. 3.6. The details of the calculations have been described in Chapter 2.

### 3.1 Lane order parameter

On application of the applied field with strength  $f$ , system reaches steady states. Fig. 3.1 (a-c) show transverse plane snapshots for field strength  $f = 50$ ,  $f = 150$  and  $f = 300$  respectively. Typical particle configurations in a typical strip in XZ plane in Fig. 3.1 (d-f) for the three values of  $f$ . Snapshots [Figs. 3.1(a,d)] show homogeneously mixed opposite-charges dispersed in the system for  $f = 50$ . With increasing  $f$ , the pairs takes the form of tiny domains of likely charges with short-ranged structural order[Figs. 3.1(b)]. These domains tend to align along  $f$  in [Fig. 3.1(e)]. Increasing  $f$  further, the domains coarsen to network-like structure in XY plane with long-range correlation [Fig. 3.1(c)]. The structures proliferate in the direction of the  $f$  as lanes for  $f = 300$  [Fig. 3.1(f)].

In the equilibrium states, the lane order parameter (Sec. 2.3.1)  $\Phi = \Phi_{Eq} \approx 0.56$ . As soon as the field is turned on,  $\Phi$  monotonically increase and reaches a steady value  $\Phi_S$ . In steady states,  $\Phi$  fluctuates around  $\Phi_S$ .  $\Phi_S$  though depends upon the  $f$ .  $\Delta\Phi = \Phi(f) - \Phi_{Eq}$  is the tendency of laning in the system for a particular value of  $f$ . Here,  $\Delta\Phi = 0$  for  $f = 0$ .  $\Delta\Phi \approx 0$  retains upto  $f = 50$ . We observe  $\Delta\Phi \neq 0$  for  $f \geq 50$ . Beyond this  $\Delta\Phi$  monotonically increase with  $f$  [Fig. 3.2].

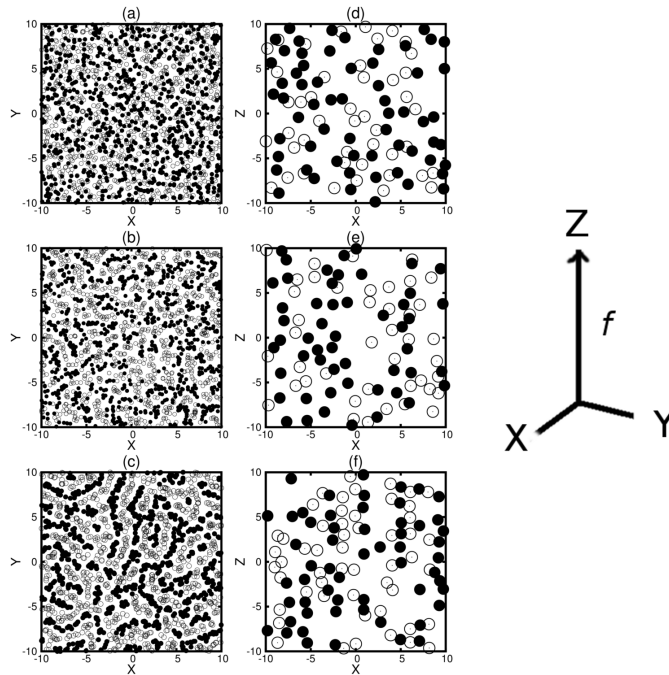


Figure 3.1: Snapshots of particles ( positively charged colloidal particles, Filled circle and negatively charged colloidal particles, circle with  $N_+ + N_- = N = 2N_+ = 2N_- = 2000$ ) in XY plane (a) for  $f = 50$  (b)  $f = 150$  and (c)  $f = 300$ . Typical particle configurations in XZ plane for  $9.5 < Y < 10.5$  are shown (d) for  $f = 50$  (e)  $f = 150$  and (f)  $f = 300$ .

## 3.2 Density Profiles

We substantiate the particle configurations in Fig. 3.2 through the density plots. Both species behave similarly, and we focus on the +ve species.  $\rho^{(+)}(Y, Z)$ ,  $\rho^{(+)}(X, Z)$  and  $\rho^{(+)}(X, Y)$  represent density profiles of the +ve species in YZ, XZ and XY planes respectively. For  $f = 0$ , the mixture is homogeneous and we observe  $\rho^{(+)}(X, Y) \approx \rho^{(+)}(X, Z) \approx \rho^{(+)}(Y, Z)$ . We show  $\rho^{(+)}(X, Y)$  and  $\rho^{(+)}(X, Z)$  in Fig.3.3 for different  $f$ . For small  $f$ (= 50), a nearly homogeneous mixed phase is obtained, where small domains of like-charged particles aligned parallel to the field is observed [Figs. 3.3(a) and (b)]. These structures are similar to that for  $f = 0$ . With increase in  $f$ , the difference in the structural morphology in XY and XZ becomes more prominent. Bigger domains are seen in  $\rho^{(+)}(X, Y)$  with increasing  $f$ (= 150) [Figs. 3.3(c) and (d)]. Finally the lane state takes place, as in earlier observations [16, 17], for sufficiently large  $f$  (= 300). Here networks of large domains in XY plane along with vertical lanes in the XZ plane are seen [Figs. 3.3(e) and (f)]. The structural morphologies in XY plane are very similar to those in pattern forming liquids [9]. Our primary focus would be on the transverse plane

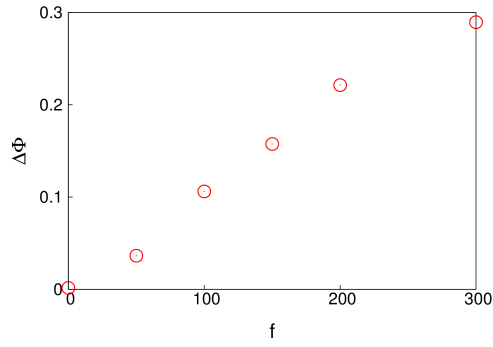


Figure 3.2: Dependence of Lane Order parameter  $\Delta\Phi = \Phi(f) - \Phi(0)$  on  $f$ .

where structural changes are significant.

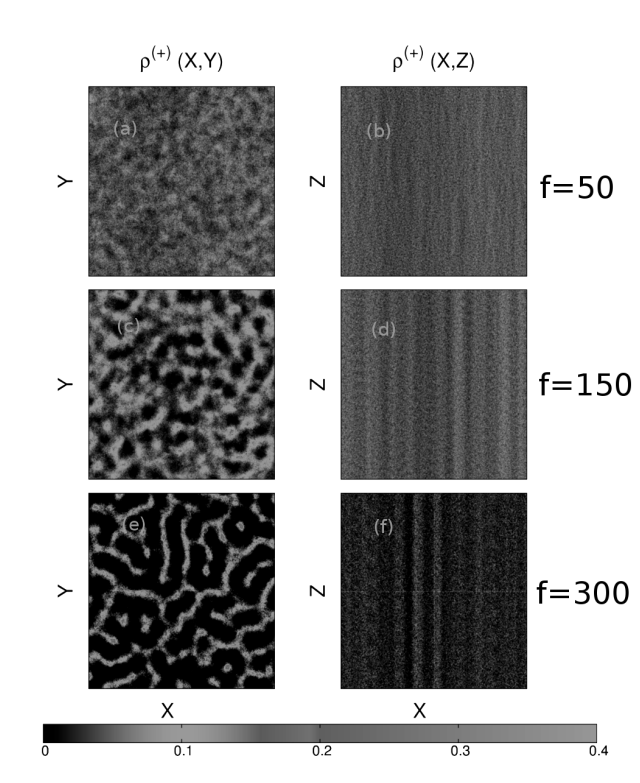


Figure 3.3: Density Plots (a)  $\rho^{(+)}(X,Y)$  and (b)  $\rho^{(+)}(X,Z)$  for  $f=50$ ; (c)  $\rho^{(+)}(X,Y)$  and (d)  $\rho^{(+)}(X,Z)$  for  $f=150$ ; and (e)  $\rho^{(+)}(X,Y)$  and (f)  $\rho^{(+)}(X,Z)$  for  $f=300$ . The contour values are indicated by the shades at the bottom

### 3.3 Pair Correlation Function

The steady state structures are characterized via the pair correlation functions. The pair correlation function, between two like charges,  $g_f^{(++)}(r_{\perp}, z)$  and that between two opposite charges,  $g_f^{(+-)}(r_{\perp}, z)$  are shown in Fig.3.4 as functions of  $r_{\perp}$  for two representative values of

$z$ . We observe correlations only upto single particle diameter for  $f=50$  for both values of  $z$  [Inset, Fig.3.4(a)]. At  $f=150$  [Main panel, Fig. 3.4(a)], the correlations in  $g_f^{(++)}(r_\perp, z)$  extend up to a couple of coordination shells for both  $z$ . The strong peak in  $g_f^{(+-)}(r_\perp, z)$  for  $r_\perp \approx 1$  indicates tendency of alignment of positively charged particles in vertical lanes with short ranged correlations in the transverse plane in the pre-lane state. Fig.3.4(b) shows PCFs for fully developed lane state with enhanced in-plane correlations extending upto several particle diameter at higher  $f$  ( $=300$ ) for both  $z$ . Thus length scale of structural correlations increases with  $f$ .

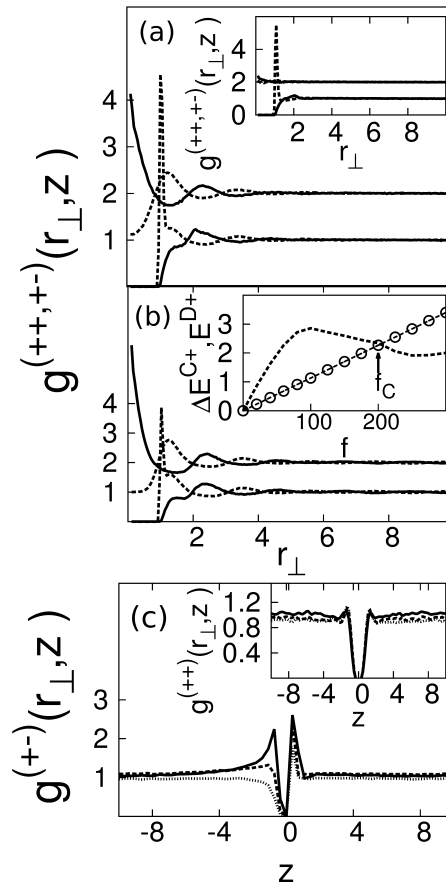


Figure 3.4: Structural Correlations:  $g_f^{(++)}(r_\perp, z)$  (solid line) and  $g_f^{(+-)}(r_\perp, z)$  (dashed line) as functions of  $r_\perp$  for  $z=0$  (lower curves) and  $z=10.7$  (upper curves, with vertical offset 1.0) for (a)  $f=150$  and Inset,  $f=50$  and (b)  $f=300$  (main panel). Inset,  $\Delta E^{C+}(f)$  (dashed line) and  $E^{D+}(f)$  (open circles) as functions of  $f$ . Dependences of (c)  $g_f^{(+-)}(r_\perp, z)$  (main panel) and  $g_f^{(++)}(r_\perp, z)$  (Inset) on  $z$  at  $r_\perp \approx 1$  for  $f=50$  (solid line),  $f=150$  (dashed line) and  $f=300$  (dotted line).

We show  $g_f^{(+)}(r_\perp, \pm z)$  (Main panel) and  $g_f^{(++)}(r_\perp, \pm z)$  (Inset) in Fig. 3.4(c) as functions of  $z$  at  $r_\perp \approx 1$  for different values of  $f$ . For  $f = 0$ ,  $g_f^{(\pm)}(r_\perp, z) \approx g_f^{(\pm)}(r_\perp, -z)$  (data not shown). For  $f \neq 0$ , the symmetry in  $g_f^{(+)}(r_\perp, z)$  is lost, although  $g_f^{(++)}(r_\perp, z)$  remains symmetric. For  $f = 50$ , there are unequal peaks in  $g_f^{(+)}(r_\perp, z)$  at  $z \approx \pm 1$ . This peak gets broadened at  $f = 150$ . For  $f = 300$ ,  $g_f^{(+)}(r_\perp, -z)$  decays as  $(-z)^{-\gamma}$  with  $\gamma \approx 2.09$ . This algebraic decay is consistent to the observations reported for two dimensional systems [22].

The correlation energy [38]  $E^{C+}(f) (= \int V^{(++)}(r) g_f^{(++)}(r_\perp, z) d^2 r_\perp dz + \int V^{(+)}(r) g_f^{(+-)}(r_\perp, z) d^2 r_\perp dz)$  is the cost of energy for replacing a negatively charged particle by a positively charged particle in a domain of positively charged particles. Inset, Fig. 3.4(b) shows the correlation energy  $\Delta E^{C+} = E^{C+}(f) - E^{C+}(0)$  and energy due to the external electric field,  $E^{D+}(f) = 2fq \int_0^{L/2} z \rho(z) dz$  as functions of  $f$ .  $\Delta E^{C+}$  increase and peaks around  $f \approx 80$ , then it decays slowly with increasing  $f$  while  $E^{D+}$  increase monotonically with  $f$ . The correlation energy between the particles experience competition with the applied field. The energy cost of bringing like charges in a domain is compensated by the external electrostatic energy above  $f_C = 200$ .

In the transverse plane, the effective interaction ( $V_{eff}^{(++)}(r_\perp)$ ) between a pair of  $+ve$  particles in presence of other particles is given by the relation:  $g^{(++)}(r_\perp) \sim \exp(-\beta V_{eff}^{(++)}(r_\perp))$ . This leads to  $V_{eff}^{(++)}(r_\perp) \sim -\beta \ln g^{(++)}(r_\perp)$  [38]. Similarly,  $V_{eff}^{(+)}(r_\perp) \sim -\beta \ln g^{(+)}(r_\perp)$ . In Fig. 3.5(a) we show the dependence of  $V_{eff}^{(+)}(r_\perp)$  (Main Panel) and  $V_{eff}^{(++)}(r_\perp)$  (Inset) on  $r_\perp$ . For  $f \neq 0$ , we observe a peak in  $V_{eff}^{(+)}(r_\perp)$  and a dip in  $V_{eff}^{(++)}(r_\perp)$  for  $r_\perp \approx 0$  that grows with increasing  $f$ . This indicates that with increasing  $f$ , the system experiences an enhanced effective attraction between like charge-pairs while an increased effective repulsion between oppositely charged pairs.

### 3.4 Cluster-size distribution

We compute the probability of a particle to be a part of a particular cluster of size  $s$ . In a cluster of likely charged particles, we subsequently add particles of the same species within a critical separation [42] in three dimensions (See Sec. 2.3.1),  $r_{cl}^{(++)}$  (for  $+ve$  particles) and  $r_{cl}^{(--)}$  (for  $-ve$  particles) to obtain the size of the cluster  $s$ . This is repeated for all the particles of the same charge to obtain the cluster size distribution. The probability distribution of the cluster sizes  $s$ ,  $P_{cl}(s)$  is computed for a particular value of  $r_{cl}^{(\pm\pm)} (= 1.4\sigma)$ . We plot  $P_{cl}(s)$  for the  $+ve$  charges for  $r_{cl}^{(\pm\pm)} (= 1.4\sigma)$  as a function of  $s$  for different  $f$  in Fig. 3.5(b). For  $f = 0$ ,  $P_{cl}(s)$  shows high peak at  $s = 1$  indicating isolated clusters. The situation remains somewhat similar

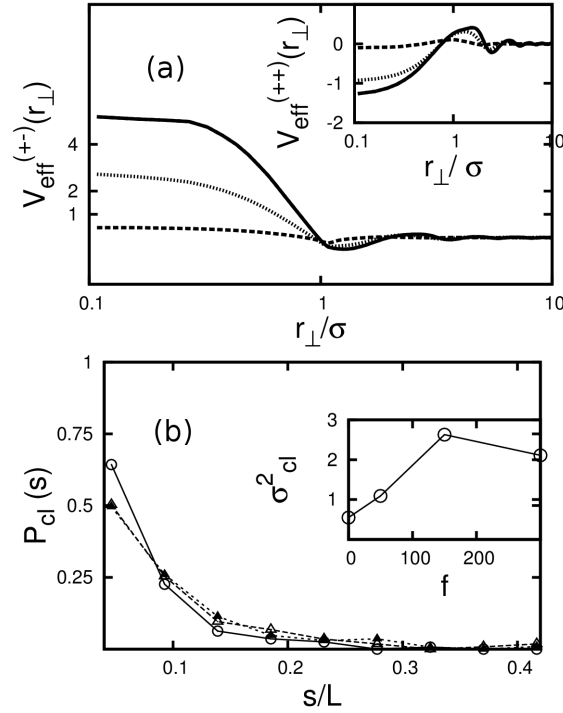


Figure 3.5: (a) Effective Interactions:  $V_{eff}^{(+)}(r_{\perp})$  vs  $r_{\perp}$  for  $f = 50$  (dashed line), 150 (dotted line) and 300 (bold line) Inset:  $V_{eff}^{(++)}(r_{\perp})$  vs  $r_{\perp}$  for  $f = 50$  (dashed line), 150 (dotted line) and 300 (bold line) (b) Dependence of  $P_{cl}(s)$  on  $s/L$  for  $f = 50$  (open circles with solid line), 150 (filled triangles and dot-dashed line), 300 (open triangles and dotted line). Lines are guide to the eyes. Inset.  $\sigma_{cl}^2$  vs  $f$  plot.

for  $f = 50$  when the system is mostly spanned by small clusters. However, for both  $f = 150$  and  $f = 300$ , the initial peak in  $P_{cl}(s)$  decreases while the probability increase for higher  $s$ . Average number of attached neighbors  $\langle \xi_{cl} \rangle \sim \int (s-1)P_{cl}(s-1)ds$  excluding the reference particle. The spread in the distribution is given by  $\sigma_{cl}^2 = \langle \xi_{cl}^2 \rangle - \langle \xi_{cl} \rangle^2$ . In Inset Fig.3.5(b), with increasing  $f$ ,  $\sigma_{cl}^2$  show a maximum at  $f = 150$ .

### 3.5 Discussion

The tendency in laning is captured via a lane order parameter which show monotonic rise with increasing field. The single point density plots show the presence of tiny lanes in the pre-lane state. With increasing field strength, the tiny lanes grow and form lanes of like charges along the field. The projection of the lanes in the transverse plane show network like structures. The pair correlation functions quantifies the ordering of these structures. The pair correlation functions

in the transverse plane show sharp peak at short distance between the opposite charges and a bulge peak among the particles with same charge at a relatively larger separation. For higher field strength, higher coordination shells appear indicating increase in particle correlations. These correlation functions are asymmetric in  $z$  and show a power-law decay along the opposite direction of the field in agreement to observations in Ref. [22]. The correlation energy dominates over the energy contribution due to the applied field for small field while the lanes are present in the system, the drift energy overcomes the correlation energy. Hence, the particles align in lanes along the field for larger strength of the field. Thus, the effective interaction mediated by the like particles show attraction at short range while repulsion between the opposite charges. The spread in the cluster size distribution show non-monotonic dependence on the field.

### 3.6 Conclusion

In this chapter, we consider the microscopic structures in the steady states. In the equilibrium, the system is homogeneous. The applied field drives the system away from its equilibrium to non-equilibrium steady states. The system crosses over from homogeneous liquid to state with patterns: For sufficiently large strength, the systems reaches lane state with network like structures in the transverse plane proliferated along the field while for intermediate strength, the system reaches pre-lane state with relatively smaller domains in the transverse plane forming tiny lanes. This sets our follow up dynamic analysis in three regimes: the homogeneous state where the electrostatic energy dominates regime and field dominated lane state and, in between a regime of *pre-lane* state where the both competes.

# Chapter 4

## Dynamical Response in Steady States

We explore dynamic responses in terms of self-vHfs and distinct-vHf and relate them to the underlying structural morphology in non-equilibrium steady states [23] described in Chapter 3. Here, we base our analysis of single particle dynamics using the self-vHf (Sec. 4.1). We also explore the particle resolve dynamics in Sec. 4.2. In Sec. 4.3, we discuss our results on distinct-vHfs. We discuss our results in Sec. 4.4 and conclude in Sec. 4.5.

### 4.1 Self van Hove functions

We focus on the self-vHfs to explore the single particle dynamics. We find that in presence of non-zero  $f$ ,  $G_S^{(\pm)}(\Delta z, t) \neq G_S^{(\pm)}(-\Delta z, t) \neq G_S^{(\pm)}(\Delta r_{\perp}, t)$  where  $\Delta r_{\perp} = |\Delta \vec{r}_{\perp}|$ . The peaks in  $G_S^{(\pm)}(\pm\Delta z, t)$  shift linearly in  $t$  with slope  $v_d \approx qf/\Gamma$ . We account for drift velocity,  $v_d$  by transforming to  $\Delta z' = \Delta z - v_d t$ . In Fig. 4.1, we show the dependence of  $G_S^{(+)}(\Delta z', t)$  on  $\pm\Delta z'$  for different  $f$ . For all  $f$ ,  $G_S^{(+)}(-\Delta z', t)$  is Gaussian. In contrast,  $G_S^{(+)}(\Delta z', t)$  behaves differently:  $G_S^{(+)}(\Delta z', t)$  is Gaussian for  $f = 50$  [Fig. 4.1(a)], while it has an exponential tail for  $f = 150$  [Fig. 4.1(b)] close to  $f_c$ . Increasing  $f (= 300)$  further,  $G_S^{(+)}(\Delta z', t)$  takes the form of a double Gaussian [Fig. 4.1(c)].

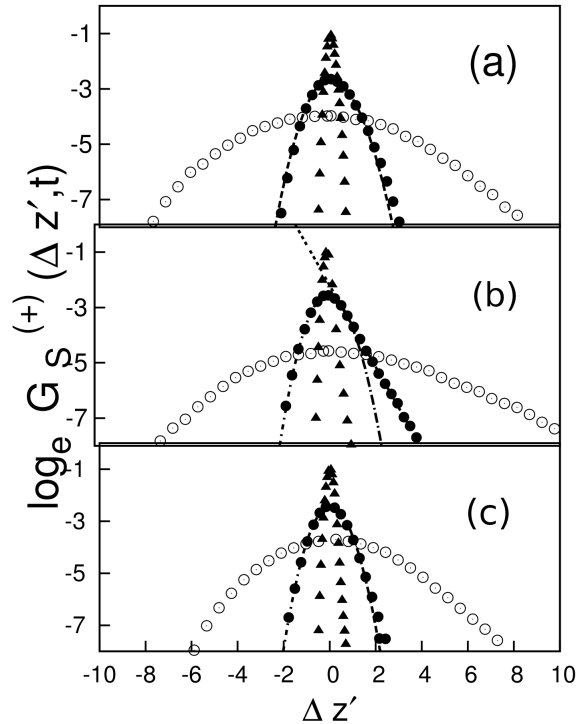


Figure 4.1:  $\ln G_S^{(+)}(\Delta z', t)$  vs  $\Delta z'$  for (a)  $f = 50$  (b)  $f = 150$  and (c)  $f = 300$  for  $t = 0.1\tau_\beta$  (filled triangles),  $1.0\tau_\beta$  (filled circles),  $10.0\tau_\beta$  (open circles). Exponential (dashed) and Gaussian (dot-dashed) lines are the fitted curves.

In the transverse plane,  $G_S^{(+)}(\Delta r_\perp, t)$  behaves similarly as  $G_S^{(+)}(\Delta z', t)$ . For small  $f(=50)$ ,  $G_S^{(+)}(\Delta r_\perp, t)$  is Gaussian as shown in Fig. 4.2(a). We find spatially exponential decay tail in  $G_S^{(+)}(\Delta r_\perp, t)$  as in  $G_S^{(+)}(\Delta z', t)$  for  $f = 150$  [Fig. 4.2(b)]. The amplitude of the Gaussian part relative to that of the exponential tail for large  $t$  approaches the ratio  $\Phi(f)/(1 - \Phi(f))$  given in Sec. 3. 1. This implies that exponential tail develops due to movement of  $+ve$  particles in the neighborhood of  $-ve$  particles. Anomalies in self-vHfs have been reported earlier in systems with competing time scales [44]. Heterogeneous density relaxation in our system is not ruled out due to formation of domains where the particles near the domain boundary may behave differently from those inside the domain. The self-vHfs have Gaussian form with double peaks for  $f (= 300 > f_C)$  in the fully developed lane phase [Fig. 4.2(c)].

We quantify self-vHf in the transverse plane where structural morphology undergoes distinct changes shown in Fig. 3.3. We quantify the self-vHfs as follows: The changes in the self-vHf take place at critical values,  $\Delta r_\perp = r_c$ . We fit the data to a form,  $\exp(-(\Delta r_\perp)^2/\sigma_\perp^2(t))$  for  $\Delta r_\perp < r_c$  and  $\exp(-\Delta r_\perp/\lambda_\perp(t))$  for  $\Delta r_\perp > r_c$  for  $f = 150$ . We restrict our data upto time window

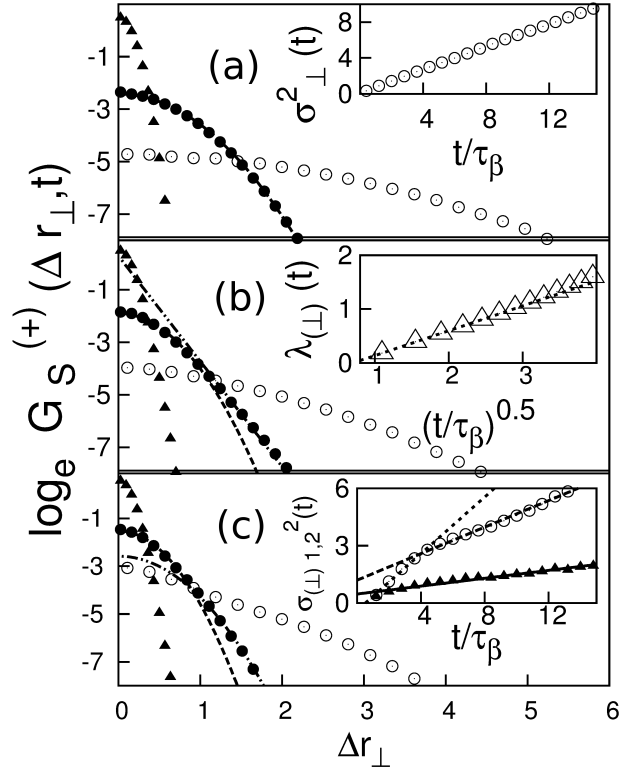


Figure 4.2: Transverse plane Self-vHfs:  $\ln G_S^{(+)}(\Delta r_{\perp}, t)$  vs  $\Delta r_{\perp}$  plots for  $t = 0.1\tau_{\beta}$  (filled triangles),  $1.0\tau_{\beta}$  (filled circles),  $10.0\tau_{\beta}$  (open circles): (a)  $f = 50$ ; dashed line: Gaussian fit. Inset:  $\sigma_{\perp}^2(t)$  as a function of  $t$  (b)  $f = 150$ ; dashed line: Gaussian and dot-dashed line: exponential tail. Inset:  $\lambda_{\perp}(t)$  as a function of  $t$  (triangles), dotted line shows  $\lambda_{\perp}(t) \sim (\frac{t}{\tau_{\beta}})^{0.5}$ . (c)  $f = 300$ ; dashed line and dot-dashed line: double Gaussian fits. Inset: Dependences of  $\sigma_{\perp(1)}^2(t)$  (filled symbols) and  $\sigma_{\perp(2)}^2(t)$  (open symbols) on  $t$ . Lines show the best fitted linear curves.

$t \approx 15\tau_{\beta}$  so that the noisy part of the very long time interval is avoided in the fitting. We fit  $G_S^{(+)}(\Delta r_{\perp}, t) = A \exp(-(\Delta r_{\perp})^2/\sigma_{\perp}^2(t))$  for  $\Delta r_{\perp} < r_c(t)$  and  $G_S^{(+)}(\Delta r_{\perp}, t) = B \exp(-\Delta r_{\perp}/\lambda_{\perp}(t))$  for  $\Delta r_{\perp} > r_c(t)$ . We minimize  $\chi^2$  with respect to  $r_c$  and the fitting parameters. The fitting for other values of  $f$  has also been done similarly. The data fitting for  $f = 300$  has been done by double Gaussians with width parameters  $\sigma_{\perp(1)}^2(t)$  for  $\Delta r_{\perp} < r_c$  and  $\sigma_{\perp(2)}^2(t)$  for  $\Delta r_{\perp} > r_c$ . We find that  $r_c$  decreases with  $t$ , but saturates to a finite value for at least two decades, implying that the deviations of dynamical behaviors from normal liquid persist till very long time.

The fitted curves are shown for representative cases in insets Fig. 4.2. Inset, Fig.4.2(a) shows that  $\sigma_{\perp}^2(t)$  depends linearly on  $t$  as in normal liquids for  $f = 50$ . Inset, Fig. 4.2(b) shows  $\lambda_{\perp}(t) \sim t^{0.5}$ . On the other hand,  $\sigma_{\perp}^2(t) \sim t$  (data not shown) for  $f = 150$ . This is characteristic of non-Fickian diffusion [44]. The slopes of  $\sigma_{\perp(1)}^2(t)$  and  $\sigma_{\perp(2)}^2(t)$  for  $f = 300$

show linear dependences on  $t$  [ Inset, Fig. 4.2(c)]. Our data indicate presence of two diffusion coefficients for  $f = 300$ .

## 4.2 Particle resolved picture

The exponential tail has been phenomenologically described in terms of heterogeneity in diffusion [44]. In order to gain microscopic understanding of the dynamic behavior, we pick up 40 particles among the  $+ve$  charged particles in the system [49]. The individual particles are tracked and probability distribution of particle distributions,  $P^{(+)(i)}(\Delta r_{\perp}, t)$  of tagged  $+ve$  particles are computed for each of the tracked particles. The second moments in  $P^{(+)(i)}(\Delta r_{\perp}, t)$ ,  $\sigma_{(i)}^2(t) = \int \Delta r_{\perp}^2 P^{(+)(i)}(\Delta r_{\perp}, t) d^2(\Delta r_{\perp})$ , are shown in Fig. 4.3(a) for  $f = 50$ ,  $f = 150$  and 300 respectively. We find different slopes for different particles in the given time window. The slopes give the self diffusion coefficients,  $D_r$  of the tagged particles.

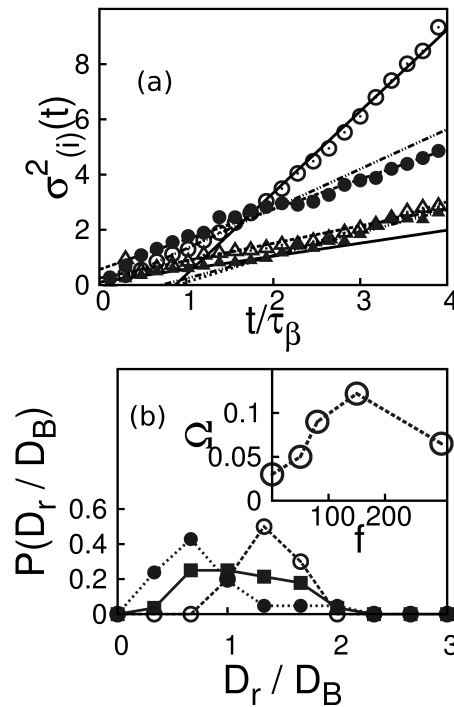


Figure 4.3: (a)  $\sigma_{(i)}^2(t)$  vs  $t$  plots for two randomly tagged particles for  $f = 150$  (open symbols) and  $f = 300$  (filled symbols). (b)  $P(\frac{D_r}{D_B})$  vs  $\frac{D_r}{D_B}$  plots for  $f = 50$  (dotted line with open circles), 150 (solid line with filled squares) and 300 (dotted line with filled circles) Inset:  $\Omega$  as a function of  $f$ . The dotted line is guide to the eyes.

The diffusivities are collated to obtain the diffusion spectrum,  $P(D_r/D_B)$ . Fig.4.3(b) shows

the distribution  $P(D_r/D_B)$  where  $D_B$  is the bulk diffusion coefficient. We observe a sharp peak in  $P(D_r/D_B)$  for  $f = 50$  at  $D_r \approx 1.3D_B$  indicating increase in average diffusion in the transverse plane. The distribution is much broader for  $f = 150$  suggesting the possibility of multiple close diffusive regimes in the system.  $P(D_r/D_B)$  gets sharp again at  $f = 300$ . There exists a fast diffusion tail indicating low probability of fast particles in the system. However, the peak in  $P(D_r/D_B)$  shifts to lower values of  $D_r$  ( $\approx 0.7D_B$ ) which affirms slowing down in the system due to increasing structural heterogeneity in presence of the field. In order to quantify the heterogeneity in dynamical response we take the width of  $P(D_r/D_B)$  around the peak,  $\Omega$ , as a measure of heterogeneity in diffusion.  $\Omega$  has a maximum around  $f = 150$  [Inset. Fig. 4.3(b)]. The mean diffusion,  $\langle D \rangle (= \int DP(D)dD) \approx 1.3D_B$  for  $f = 50$ . However,  $\langle D \rangle$  is ill-defined for  $f = 150$ .  $\langle D \rangle$  ( $\approx 0.7D_B$ ) corresponding to the peak for  $f = 300$  is lower than that for  $f = 50$ . However, the tail in  $P(D)$  for  $f = 300$  corresponds to  $\langle D \rangle \approx 2D_B$  which is higher than that for  $f = 50$ .

### 4.3 Distinct van Hove functions

We examine the distinct van Hove functions for separation  $r_\perp$  between two particles in the transverse plane to the field in time interval  $t$ . Since,  $G_D^{(++)}(r_\perp, t) = G_D^{(--)}(r_\perp, t)$  and  $G_D^{(+-)}(r_\perp, t) = G_D^{(-+)}(r_\perp, t)$ , we focus on a positively charged colloidal particle. We consider  $G_D^{(++)}(r_\perp, t)$  between two *ve* charges and  $G_D^{(+-)}(r_\perp, t)$  between a *ve* and *-ve* in steady states. At  $t = 0$ ,  $G_D^{(+\pm)}(r_\perp, 0) = g^{(+\pm)}(r_\perp)$ .

First, we look at the case for  $f = 50$  in Inset Fig. 4.4 (a). At  $t = 0$ ,  $G_D^{(++)}(r_\perp, t)$  has a kink at  $r_\perp \approx 2.2$  which disappear at  $t = 10$ . For  $G_D^{(+-)}(r_\perp, t)$ , the peak is sharper and located at  $r_\perp \approx 1.1$  at  $t = 0$ . This peak flattens very rapidly with  $t$  and disappear at  $t = 10\tau_\beta$ . For  $f = 150$ , both  $G_D^{(++)}(r_\perp, t)$  and  $G_D^{(+-)}(r_\perp, t)$  show few coordination shells at  $t = 0$  which decays at  $t = 10$  [Fig. 4.4(a)]. The peaks in both  $G_D^{(++)}(r_\perp, t)$  and  $G_D^{(+-)}(r_\perp, t)$  at  $t = 0$  shifts to higher values in  $r_\perp$  for  $f = 300$  and persists ( $t = 10\tau_\beta$ ). Higher coordination shells are seen in both the cases at both  $t = 0$  and  $t = 10\tau_\beta$  [Fig. 4.4(b)].

The wave-vector ( $q_\perp$ ) dependent distinct-vHfs,  $G_D^{(+\pm)}(q_\perp, t)$  are obtained by taking a Fourier transform of  $G_D^{(+\pm)}(r_\perp, t)$  for each  $t$ .  $G_D^{(++)}(q_\perp, t)$  show a maximum at  $q_\perp \approx q_0$  and  $G_D^{(+-)}(q_\perp, t)$  has a dip at  $t = 0$ . With increasing  $t$ , both the peak and the dip decays. We show the evolution of both  $G_D^{(++)}(q_\perp, t)$  and  $G_D^{(+-)}(q_\perp, t)$  for  $f = 150$  as a function of  $q_\perp$  at  $t = 0$  and  $t = 10\tau_\beta$  in Fig. 4.5(a). In order to obtain the structural relaxation, we track the decay of the peak in  $G_D^{(++)}(q_\perp, t)$  and dip in  $G_D^{(+-)}(q_\perp, t)$  with  $t$ . We quantify this by  $C_0^{(++)}(t) [= \frac{G_D^{(++)}(q_0, t) - 1}{G_D^{(++)}(q_0, t=0) - 1}]$

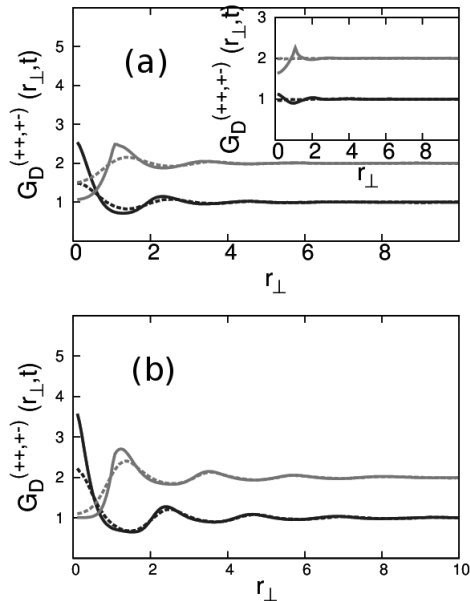


Figure 4.4: (a)  $G_D^{(+++)}(r_\perp, t)$  (lower curves) and  $G_D^{(+-)}(r_\perp, t)$  (upper curves, with vertical offset 1.0) as functions of  $r_\perp$  for  $t = 0$  (solid line) and  $t = 10\tau_\beta$  (dashed line) for (a)  $f = 50$  (Inset),  $f = 150$  (main panel) and (b)  $f = 300$

and  $C_0^{(+)}(t) [= \frac{1-G_D^{(+)}(q_0, t)}{1-G_D^{(+)}(q_0, t=0)}]$ . We show these quantities in Fig. 4.5(b) in semi-logarithmic plots. The plots show that the relaxation of  $+ve$  particles in the neighbourhood of other  $-ve$  particles (denoted by  $C_0^{(+)}(t)$ ) is slower than that in the vicinity of other  $+ve$  particles (denoted by  $C_0^{(++)}(t)$ ). We observe that the decay is exponential in  $t$  in general indicating diffusive relaxation [38], except for,  $-\ln C_0^{(+)}(t) \sim t^{0.75}$  for  $f = 150$ , implying a slow stretched exponential relaxation.

The slow relaxation could be understood as follows: The Vineyard approximation [38, 50] implies that,  $G_D^{(+\pm)}(q_0, t) \approx G_S^{(+)}(q_0, t)S^{(+\pm)}(q_0)$  where  $S^{(+\pm)}(q_0)$  are the structure factors, the fourier transforms of the respective PCFs. Here,

$$C_0^{(+\pm)}(t) \approx G_S^{(+)}(q, t), \quad (4.1)$$

for all  $q$ . Here,  $G_S^{(+)}(q, t) = \int G_S^{(+)}(r, t)e^{iq \cdot r} d\vec{r}$ . Since  $S^{(+\pm)}(q_0)$  does not depend on  $t$ , the time dependence of  $C_0^{(+\pm)}(t)$  will come from  $G_S^{(+)}(q_0, t)$  which we analyze here. Our simulations indicate that  $G_S^{(+)}(q_0, t) = G_S^{(N)}(q_0, t) + \frac{\Phi}{1-\Phi}G_S^{(T)}(q_0, t)$ . Let us consider,  $C_0(t) \equiv C_0^{(+\pm)}(t) \approx G_S^{(+)}(q, t)$

Let,

$$\ln C_0(t) = G_S^{(N)}(q_0, t) - C_r(t) \quad (4.2)$$

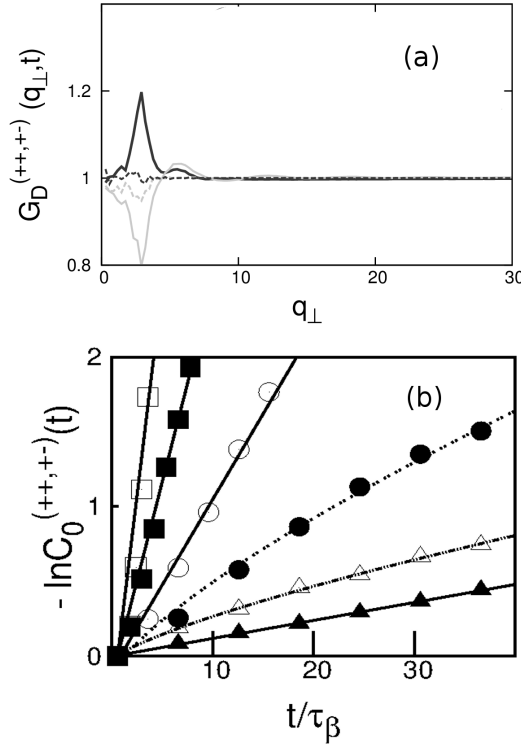


Figure 4.5: Dependences of  $G_D^{(+++)}(q_\perp, t)$  (upper curves, with vertical offset 0.1) and  $G_D^{(+,-)}(q_\perp, t)$  (lower curves) on  $q_\perp$  for  $f = 150$  for  $t = 0$  (solid line) and  $t = 10\tau_\beta$  (dashed line). (b) Dependences of  $-\ln C_0^{(+++)}(t)$  (open symbols) and  $-\ln C_0^{(+,-)}(t)$  (filled symbols) on  $t/\tau_\beta$  for  $f = 50$  (squares),  $f = 150$  (circles) and  $f = 300$  (triangles). Lines show the fitted curves.

where  $G_S^{(N)}(q_0, t)$  is the Gaussian component and  $C_r(t)$  is a correction due to the tail in  $G_S(q_0, t)$

Taking logarithm on both sides and assuming the correction be small, one can write to the first order,

$$C_0(t) \approx G_S^{(N)}(q_0, t) - \frac{C_r(t)}{G_S^{(N)}(q_0, t)}. \quad (4.3)$$

One can as well write,

$$\ln C_0(t) \approx \ln G_S^{(N)}(q_0, t) + \ln \left[ 1 + \frac{\Phi}{1 - \Phi} \frac{G_S^{(T)}(q_0, t)}{G_S^{(N)}(q_0, t)} \right] \quad (4.4)$$

Comparing (4.3) and (4.4) we obtain,

$$-C_r(t) \sim \frac{\Phi}{1 - \Phi} G_S^{(T)}(q_0, t) \quad (4.5)$$

In 2 Dimensions,

$$G_S^{(T)}(q_0, t) \sim \int_{r_c}^{\infty} e^{-r/\lambda(t)} J_0(q_0 r) r dr \quad (4.6)$$

Substituting  $\zeta = r/\lambda$  and using  $J_0(q_0 r) \sim \frac{1}{\sqrt{q_0 r}}$  in (4.6) one gets,

$$G_S^{(T)}(q_0, t) \sim \lambda^{3/2}(t) \int \zeta^{-1/2} e^{-\zeta} d\zeta \quad (4.7)$$

Here, the  $\zeta$  integral gives a constant and using  $\lambda(t) \sim t^{0.5}$ , we get  $C_r(t) \sim t^{0.75}$  so that

$$-\ln C_0(t) \sim t^{0.75}. \quad (4.8)$$

## 4.4 Discussion

Dynamic slowing down has been observed in super-cooled systems [51, 52]. However, the slow dynamics in such systems is due to caging of the particles by their neighbours [53]. In contrast, the individual particle motions here are always diffusive. However, the diffusion has heterogeneity. This heterogeneous diffusion implies the heterogeneity in transport processes. There exist complex systems, where anomalies in dynamical responses have been ascribed phenomenologically to heterogeneity in diffusion [44, 51, 54–57]. In such attempts, the diffusion spectrum has been obtained by deconvolution of the self-vHfs using Lucy iterative method [44, 58]. Here, we obtain the diffusion spectrum from single particle tracking data itself.

## 4.5 Conclusions

The single particle dynamics has been probed using different the spatio-temporal correlation functions. The lateral self vHf is asymmetric and shifts with time due to drift for non-zero field. Both lateral and transverse self-vHf crosses over from a Gaussian form in homogeneous state to double Gaussian form in the lane state via that having exponential tail in *pre-lane* state. The exponential tail is observed when the diffusion spectrum is broad. There is heterogeneity in single particle diffusion. Moreover, the tails lead to slow structural relaxation. These results can be verified by measuring vHfs through experiments using neutron scattering.

# Chapter 5

## Structural Relaxation in Steady States

The structural changes in a binary mixture of opposite charges by application of electric field are given in Chapter 3. The vHfs show heterogeneity in diffusion given in Chapter 4. Here, we extend our analysis on the structural relaxation in the steady states [26]. We discuss our analysis based on the Overlap Function and Dynamical Susceptibility (Sec. 5.1) followed by distinct vHfs between fast and slow relaxing particles (Sec. 5.2). We include a discussion in Sec. 5.3 and we conclude in Sec. 5.4. The detailed methods of our analysis is given in Chapter 2.

### 5.1 Overlap Function

The diffusion spectrum in Chapter 4 for different  $f$  indicates the slowing down in dynamics. The Overlap function has been very successfully tested in glass forming systems in explaining the slowing down. We adapt the formalism in order to analyse the slowing down. We compute self-overlaps between particle configurations in the transverse plane, separated by time  $t$ ,  $\tilde{q}_{(\perp)}^{(\pm)}(t)$  for both  $+ve$  and  $-ve$  charges respectively. Both charges behave identically, so we focus on  $\tilde{q}_{(\perp)}^{(+)}(t)$ . The probability distribution function of  $\tilde{q}_{(\perp)}^{(+)}(t)$  over different configurations is given by  $P(\tilde{q}_{(\perp)}^{(+)}(t))$ . We observe  $P(\tilde{q}_{(\perp)}^{(+)}(0)) \sim \delta(\tilde{q}_{(\perp)}^{(+)}(0) - N_+)$ . For  $t \neq 0$ , the peaks in  $P(\tilde{q}_{(\perp)}^{(+)}(t))$  shift with increasing  $t$ . In Fig. 5.1(a) we show the dependence of  $P(\tilde{q}_{(\perp)}^{(+)}(t))$  for various  $f$  for a typical  $t = 0.05\tau_\beta$ . For small  $t$ ,  $P(\tilde{q}_{(\perp)}^{(+)}(t))$  is a Gaussian. For  $f = 50$ , at  $t = 0.05$ ,  $P(\tilde{q}_{(\perp)}^{(+)}(t))$  has a peak at  $\tilde{q}_{(\perp)}^{(+)}(t) \approx 0.89$ . This peak shifts to lower values of  $\tilde{q}_{(\perp)}^{(+)}(t) (\approx 0.87)$  for  $f = 150$  and then again shifts to the higher values of  $\tilde{q}_{(\perp)}^{(+)}(t) (\approx 0.91)$  for  $f = 300$  indicating a non-monotonic trend.

The Overlap Function [41] is given as,

$$Q_{(\perp)}^{(+)}(t) \sim \int \tilde{q}_{(\perp)}^{(+)}(t) P(\tilde{q}_{(\perp)}^{(+)}(t)) d\tilde{q}_{(\perp)}^{(+)}(t). \quad (5.1)$$

For all  $f$ ,  $Q_{(\perp)}^{(+)}(0) = 1$  and they decay monotonically with  $t$  [Fig. 5.1(b)]. However, the decay rates in  $Q_{(\perp)}^{(+)}(t)$  vary with the strength of  $f$ .  $f = 50$  shows a relatively fast decay in  $Q_{(\perp)}^{(+)}(t)$ . The rate decrease with  $f$  indicating a slowing down in the transverse plane as in Ref. [14]. For  $f = 300$ , we observe that  $Q_{(\perp)}^{(+)}(t) \approx 0.25$  which is twice the value ( $\approx 0.12$ ) of that for  $f = 50$  at  $t = 1.0\tau_{\beta}$ . We find an intermediate value ( $\approx 0.18$ ) in  $Q_{(\perp)}^{(+)}$  for  $f = 150$ . Also there exists a crossover in  $Q_{(\perp)}^{(+)}$ . For  $f = 50$ ,  $Q_{(\perp)}^{(+)}(t) \sim t^{\alpha}$  where  $\alpha \approx -0.86$ . We find  $Q_{(\perp)}^{(+)}(t) \sim e^{-t^{-\beta}}$  in the time window  $10\tau_{\beta} < t < 40\tau_{\beta}$  for  $f = 150$  with  $\beta \approx 0.37$ [Inset. Fig. 5.1(c)].  $Q_{(\perp)}^{(+)}(t)$  shows a power law dependence, like in aggregating liquids [45] with  $\alpha \approx -0.52$  for  $f = 300$  for  $1\tau_{\beta} < t < 20\tau_{\beta}$  (Fig. 5.1(c)).

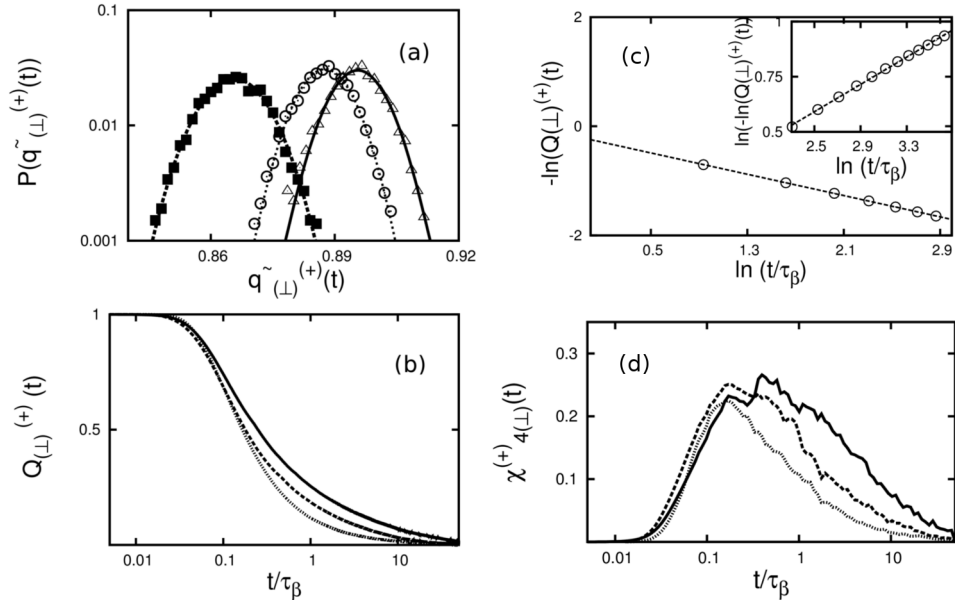


Figure 5.1: (a) Distribution of Overlaps,  $P(\tilde{q}_{(\perp)}^{(+)}(t))$  for different  $\tilde{q}_{(\perp)}^{(+)}(t)$  is shown for  $t = 0.05\tau_{\beta}$ :  $f = 50$  (open circles),  $f = 150$  (filled squares) and  $f = 300$ (open triangles). Lines show the fitted Gaussian curves. (b) Dependences of  $Q_{(\perp)}^{(+)}(t)$  on  $t$  for three regimes: fast-segregation  $f = 50$  (dotted line), mixed relaxation  $f = 150$  (dashed line) and slow relaxation  $f = 300$  (solid line) (c)  $\ln Q_{(\perp)}^{(+)}(t)$  vs  $\ln(t/\tau_{\beta})$  for  $f = 300$ . Inset.  $\ln(\ln Q_{(\perp)}^{(+)}(t))$  vs  $\ln(t/\tau_{\beta})$  for  $f = 300$  (d) Dynamical Susceptibility,  $\chi_4^{(+)}(t)$  for three regimes:  $f = 50$  (dotted line), 150 (dashed line) and 300 (solid line)

In order to understand the structural responses we compute the dynamical susceptibility,  $\chi_4^{(\pm)}(t)$  which is given in terms of the fluctuations in  $Q(t)$  [40, 41],

$$\chi_4^{(\pm)}(t) = \langle Q^{(\pm)2}(t) \rangle - \langle Q^{(\pm)}(t) \rangle^2. \quad (5.2)$$

It peaks at  $t = \tau_4$  which is proportional to the structural relaxation time,  $\tau$  [41]. We show the evolution of  $\chi_{4(\perp)}^{(+)}(t)$  with  $t$  for different  $f$  in Fig. 5.1(d). For  $f = 50$ , the peak in  $\chi_{4(\perp)}^{(+)}(t)$  shifts to lower value of  $t$  than that for  $f = 0$  indicating phase segregation due to the faster relaxation. For  $f = 150$ ,  $\chi_{4(\perp)}^{(+)}(t)$  grows and has a broad peak, showing the coexisting time-scales of structural relaxation with comparable magnitudes in the system. On increasing  $f$  further,  $\chi_{4(\perp)}^{(+)}(t)$  shows two distinct peaks for  $f = 300$  depicting heterogeneity.

In the homogeneous state, the dynamics is entirely governed by the fast particles driven by the field. The peak in  $\chi_{4(\perp)}^{(+)}(t)$  for  $f = 50$  corresponds to relaxation by the faster particles in the system. In contrast, the slow dynamics in the lane state is associated with the particles in the proliferated lanes. This results in the predominant peak in  $\chi_{4(\perp)}^{(+)}(t)$  at higher  $t$  for  $f = 300$  while the peak at lower  $t$  is entirely due to the fast particles. The dynamics in the intermediate state experiences a competition between the two. Hence, the broadening in  $\chi_{4(\perp)}^{(+)}(t)$  for  $f = 150$ . This is consistent with the data of heterogeneity in structural relaxation in the *pre-lane* state [23].

## 5.2 Relaxation of the partial structures

We find that the heterogeneity in diffusion spectrum maximized in the *pre-lane state* [See Fig. 4.3]. This indicates the possibility of multiple time-scales of relaxation due to simultaneous presence of slow and fast relaxing particles. We identify the slow and fast relaxing particles. We compute the probability distribution of square of the particle displacements,  $P(\Delta r_{\perp}^2, t)$ , in the transverse plane in a given time interval,  $t$ . We observe  $P^{(+)}(\Delta r_{\perp}^2, t) \approx P^{(-)}(\Delta r_{\perp}^2, t)$  ( $= P(\Delta r_{\perp}^2, t)$ ). At  $t = 0$ ,  $P(\Delta r_{\perp}^2, t)$  has a peak at  $\Delta r_{\perp}^2 = 0$ . We plot  $P(\Delta r_{\perp}^2, t)$  with  $\Delta r_{\perp}^2$  for  $f = 150$ (Main Panel) and  $f = 300$ (Inset) in Fig. 5.2(a). For  $t > 0$ , the the peaks in  $P(\Delta r_{\perp}^2, t)$  is located at  $\Delta r_{\perp}^2 = \Delta R_P$  with value  $\Delta P_v$ . With increasing  $t$ , we observe that the peak at  $\Delta R_P$  shifts to the higher values of  $\Delta r_{\perp}^2$  while  $\Delta P_v$  decays due to diffusion [Figs. 5.2 (b) and (c)]. The decay rates depend on the strength of  $f$ . This trend is similar to the decay of  $Q_{(\perp)}^{(+)}(t)$  and the distinct van Hove functions as in Ref. [23], affirming the increase in transverse plane slowing down in the system. In order to identify the fast and slow relaxing particles within a particular species, we tag particles as "slow relaxing" particle (S) if it has square of the displacement  $\Delta r_{\perp}^2(t) < \Delta R_P(t)$  in the time window  $t$ . Similarly we tag the particles as "fast relaxing" (F) if

$\Delta r_{\perp}^2(t) \geq \Delta R_P(t)$ . Thus we count the no F and S particles ( $N_F^{(+)}(t)$  and  $N_S^{(+)}(t)$  respectively) of  $+ve$  and  $-ve$  charges respectively in a given time interval  $t$ .

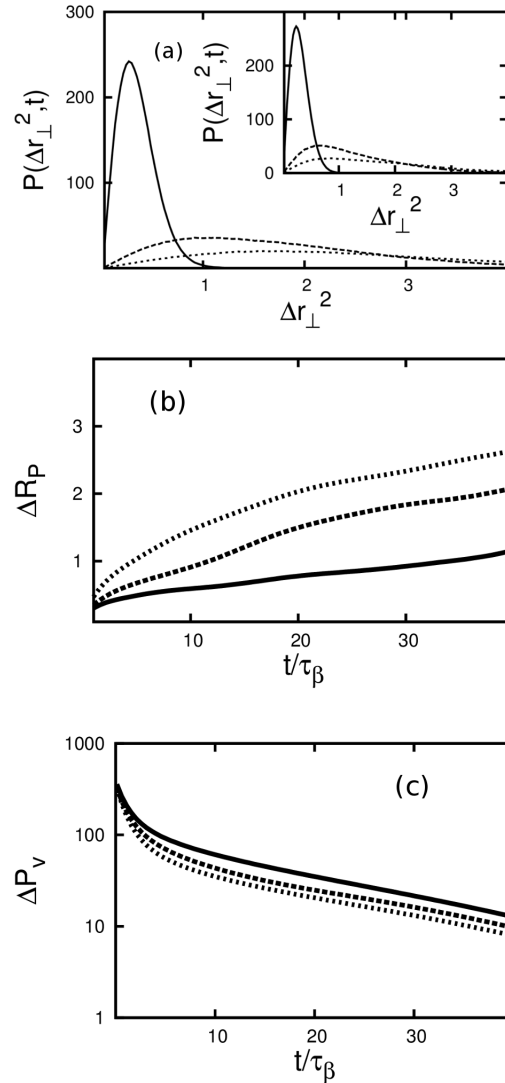


Figure 5.2: (a)  $P(\Delta r_{\perp}^2, t)$  vs  $\Delta r_{\perp}^2$  for  $t = 0.25\tau_{\beta}$ (solid line),  $12.5\tau_{\beta}$  (dashed line) and  $25\tau_{\beta}$ (dotted line) for  $f = 150$  (Main Panel) and  $f = 300$  (Inset) (b) Dependence of  $\Delta R_P$  on  $t$  for  $f = 50$ (dotted line),  $f = 150$ (dashed line) and  $f = 300$ (solid line). (c)  $\Delta P_v$  vs  $t$  for  $f = 50$ (dotted line),  $f = 150$ (dashed line) and  $f = 300$ (solid line).

Since the system consists of S and F particles of  $+ve$  and  $-ve$  charges, there exist various possibilities structural correlation between two particles can relax. For example, among  $+ve$  charged particles, the way a S particle relaxes in the vicinity of other S particles may be different to from that in the vicinity of F particles. Thus, there exists six such possibilities. We now analyze the density relaxation of these structures via different distinct van Hove functions:  $G_{D(S,S)}^{(++)}(r, t)$ ,  $G_{D(F,S)}^{(++)}(r, t)$ ,  $G_{D(F,F)}^{(++)}(r, t)$ ,  $G_{D(S,S)}^{(+-)}(r, t)$ ,  $G_{D(F,S)}^{(+-)}(r, t)$  and  $G_{D(F,F)}^{(+-)}(r, t)$ . The

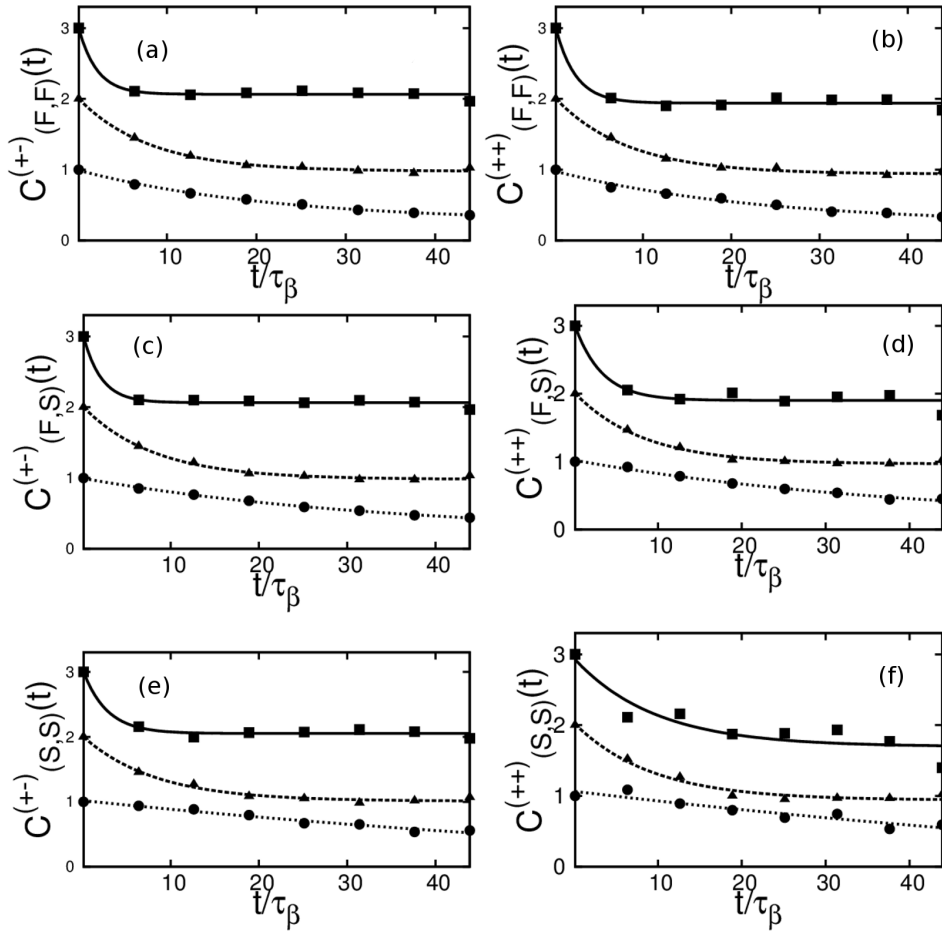


Figure 5.3: (a)  $C_{(F,F)}^{(+\pm)}(t)$ , (b)  $C_{(F,F)}^{(++)(t)}$ , (c)  $C_{(F,S)}^{(+\pm)}(t)$ , (d)  $C_{(F,S)}^{(++)(t)}$  (e)  $C_{(S,S)}^{(+\pm)}(t)$  (f)  $C_{(S,S)}^{(++)(t)}$  as a function of  $t$  for  $f = 50$  (filled squares, shown with vertical offset 2),  $f = 150$  (filled triangles, shown with vertical offset 1) and  $f = 300$  (filled circles). Solid, dashed and dotted lines show fitted lines for  $f = 50$  (shown with vertical offset 2),  $f = 150$  (shown with vertical offset 1) and  $f = 300$  respectively.

respective Fourier transforms of these quantities are given by  $G_{D(S,S)}^{(+\pm)}(q_\perp, t)$ ,  $G_{D(F,F)}^{(+\pm)}(q_\perp, t)$  and  $G_{D(F,S)}^{(+\pm)}(q_\perp, t)$ . The decay profiles of the peaks in  $G_D^{(++)(q_\perp, t)}$  and dips in  $G_D^{(+\pm)}(q_\perp, t)$  at wave vector  $q_0$  is given as

$$C_{(M,N)}^{(+\pm)}(t) = \frac{\pm G_{D(M,N)}^{(+\pm)}(q_0, t) \mp 1}{\pm G_{D(M,N)}^{(+\pm)}(q_0, 0) \mp 1} \quad (5.3)$$

as in Ref. [23]. Here  $M$  and  $N$  are indices that stand for both  $S$  and  $F$ .

We find  $C_{(M,N)}^{(+\pm)}(t) \sim \exp(-t/\tau_{(M,N)}^{(+\pm)})$  (fits are shown in Fig. 5.3(a-h)) where the timescales of relaxation are given by  $\tau_{(M,N)}^{(+\pm)}$  and are shown in the main panel of Fig. 5.4. For  $f = 50$ , we find  $\tau_{(F,F)}^{(++)} < \tau_{(F,F)}^{(+\pm)} < \tau_{(F,S)}^{(+\pm)} < \tau_{(F,S)}^{(++)} < \tau_{(S,S)}^{(+\pm)} < \tau_{(S,S)}^{(++)}$ . The trend changes for  $f = 150$  as  $\tau_{(F,S)}^{(++)} \approx \tau_{(F,F)}^{(+\pm)}$  and  $\tau_{(F,S)}^{(++)} < \tau_{(F,S)}^{(+\pm)}$ . However, these timescales are relatively close in

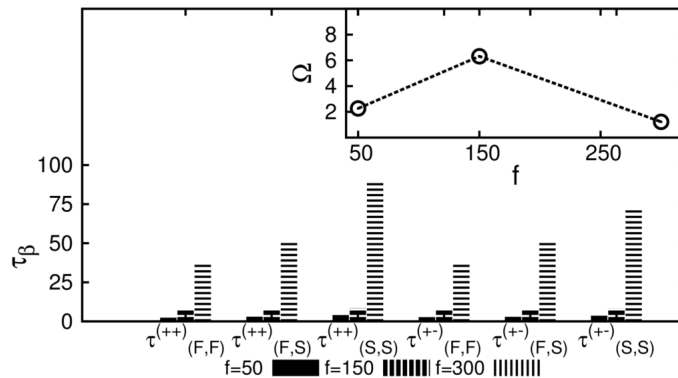


Figure 5.4:  $\tau_{(F,F)}^{(++)}$ ,  $\tau_{(F,S)}^{(++)}$ ,  $\tau_{(S,S)}^{(++)}$ ,  $\tau_{(F,F)}^{(+-)}$ ,  $\tau_{(F,S)}^{(+-)}$  and  $\tau_{(S,S)}^{(+-)}$  for  $f = 50$ ,  $f = 150$  and  $f = 300$ . Inset: Dependence of  $\Omega$  on  $f$

magnitudes. However, for  $f = 300$ , we observe  $\tau_{(F,F)}^{(++)} < \tau_{(F,F)}^{(+-)} < \tau_{(F,S)}^{(++)} < \tau_{(F,S)}^{(+-)} < \tau_{(S,S)}^{(+-)} < \tau_{(S,S)}^{(++)}$ . Here,  $\tau_{(S,S)}^{(+\pm)}$  increase significantly with increasing  $f$ . The measure of heterogeneity is given by  $\Omega = \frac{1}{(\sigma_\tau/\mu_\tau)}$  with  $\sigma_\tau^2 = \sum_{M,N} (\tau_{M,N} - \mu_\tau)^2$  and  $\mu_\tau = 1/6 \sum_{M,N} \tau_{M,N}$ , the mean relaxation time.  $\Omega$  show non-monotonic dependence on  $f$  [Inset. Fig. 5.4], like similar non-monotonic behaviour in  $\sigma_{cl}^2$ . This is also quite similar to the behavior of heterogeneity in diffusion in the same system [23].

### 5.3 Discussion

Reports [11, 20] show that the laning transition is accompanied by an initial increase in the diffusion. The increasing drift enforces the particles to move through lanes. But the particle motion in the transverse direction decrease as the bigger lanes starts to appear. This is due to the increasing effective attraction between the like charges and repulsion between the cross charges. The particles in the same lane cause the slow dynamics while the cross-lane movements are associated with faster diffusion. In the homogeneous state, the pre-dominant attraction between the opposite charges results into the faster diffusion while in the lane state, the inter-lane movements become low probable leading to a slowing down. The state for intermediate strength of the field experiences a competition between the two movements. Hence, we observe the onset of multiple time-scales in the system. This leads to anomalous dynamical responses in the *pre-lane* state [23]. We observe the separation of time-scales in the lane state via the double peaks in  $\chi_4(t)$ . The double peaks in  $\chi_4(t)$  has been previously seen in super-cooled liquids and it has been linked with short time  $\beta$ -relaxation [59] where the time-scales of the

slow and fast particles are widely separated.

## 5.4 Conclusion

In conclusion, in a driven mixture of oppositely charged colloid, we characterize slowing down accompanied by the presence of partial structures between slow and fast relaxing particles which relax at distinct rates. Earlier in super-cooled systems, possibility of such structures was predicted by Donati-Glotzar-Poole-Kob-Plimpton [60] in exploring dynamic heterogeneity which occurs when different parts of a system relaxes at different rates. The existence of these partial structures could be verified in using scattering experiments.

# Chapter 6

## Transient Response

So far we have considered the interplay between structure and dynamics in steady states in Chapter 3-5. Here we focus on the transient response as the heterogeneous steady states set in from homogeneous equilibrium state in the presence of a constant electric field [27]. We first equilibrate the system without electric field from random configurations for  $50\tau_\beta$ . Then we switch on the electric field  $f$  in  $z$ -direction to drive the system far from equilibrium. The field is kept on for  $15\tau_\beta$  so that for all  $f$  (within the observation window), the system reaches steady state. We calculate different quantities  $t_w$  time after the field is switched on. All the dynamical quantities depend on  $t_w$ . We also study the case where the field is switched off to let the system relax back to the equilibrium state. Since the system evolves with time, the averaging is done for a given time over the Brownian trajectories. This also forces us to simulate a bigger system for better statistics.

In this chapter, we discuss growth of heterogeneous structure in Sec. 6.1. The transient dynamical response and Aging in transient state have been discussed in Sec. 6.2 and 6.3 respectively. We analyze relaxation of heterogeneous structures in Sec. 6.4. We discuss our results in Sec. 6.5 and we conclude in Sec. 6.6.

### 6.1 Growth of Heterogeneous Structures

The formation of lanes are monitored via lane order parameter [17],  $\Phi(t_w)$  (See Chapter 2). In equilibrium, we observe that  $\Phi = \Phi_{Eq} \approx 0.56$  given in Chapter 3 [23]. As soon as the field is turned on, we monitor  $\Delta\Phi(t_w)(= \Phi(t_w) - \Phi_{Eq})$  with  $t_w$ . In Fig 6.1(a), we show the dependence of  $\Delta\Phi(t_w)$  on  $t_w$ . For  $f = 50$ ,  $\Delta\Phi(t_w)$  fluctuates around zero. For  $f = 150$ ,  $\Delta\Phi$  increase and reaches at a steady value  $\Delta\Phi_S \approx 0.1$  in time  $\tau_S \approx 2.4\tau_\beta$ . For  $f = 300$ , we observe a rapid increase in  $\Delta\Phi$ , approaching  $\Delta\Phi_S \approx 0.25$  with  $\tau_S \approx 1.1\tau_\beta$ .

We consider the plane transverse to the electric field which shows morphological changes in the steady states [23,26]. We focus on  $+ve$  charges, as both the species behaves similarly. The changes in structural morphology with  $t_w$  are monitored by the coarse-grained local particle distribution in the transverse plane,  $\rho^{(+)}(r_{\perp}; t_w)$  ( $= \frac{1}{N_+} \sum_{i=1}^{N_+} \delta(|\vec{r}_{\perp}(t_w) - \vec{R}_{i\perp}(t_w)|)$ ) for a given trajectory. We discuss the case of a representative trajectory. We consider three representative values of  $t_w$ :  $t_w = 0$  corresponds to the system in equilibrium,  $t_w = \frac{\tau_S}{2}$  denotes time that the system is evolving to the steady states; and  $t_w \geq \tau_S$  where the system is in steady state.  $\rho^{(+)}(r_{\perp}; t_w)$  is homogeneous for  $t_w = 0$  for all  $f$  [Fig. 6.1(b)]. For  $f = 50$ , similar homogeneous structures is retained for all  $t_w$ (data not shown). For  $f = 150$ , there are small domains at  $t_w = \frac{\tau_S}{2}$  [Fig. 6.1(c)] and form isolated bigger domains at  $t_w = \tau_S$ [Fig. 6.1(d)]. Isolated large domains are observed in  $\rho^{(+)}(r_{\perp}; t_w)$  at  $t_w = \frac{\tau_S}{2}$  for  $f = 300$  [Fig. 1(e)]. These domains proliferate to form connected domains at  $t_w \approx 2\tau_S$  [Fig. 6.1(f)].The other trajectories show similar behavior.

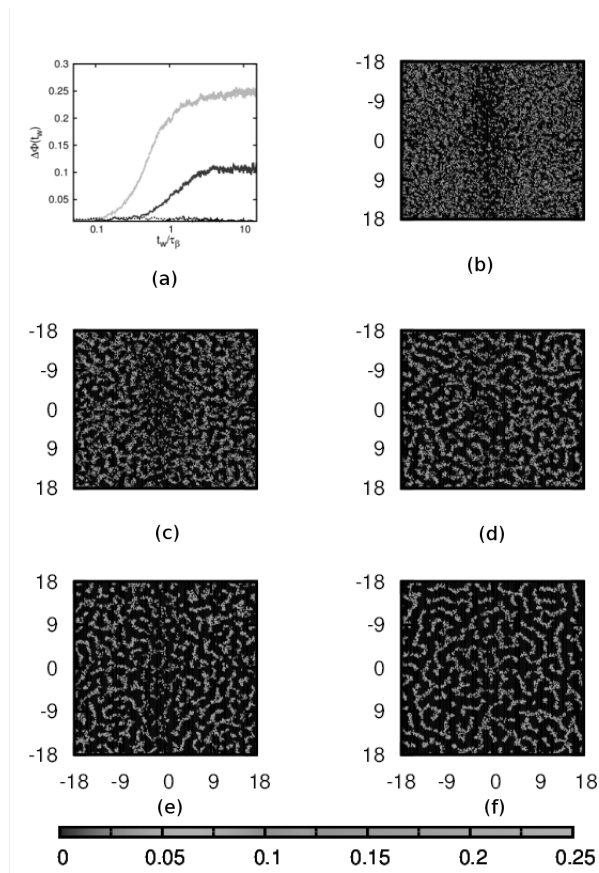


Figure 6.1: (a) Development in Laning tendency via the lane order parameter,  $\Delta\Phi$  with  $t_w$  for  $f = 50$  (dotted line),  $f = 150$  (solid line, in black) and  $f = 300$ (dashed line, in grey). (b-f)  $\rho^{(+)}(r_{\perp}; t_w)$ , for (b)  $t_w = 0$  (c)  $f = 150$ ,  $t_w = 1.2\tau_\beta$  (d)  $f = 150$ ,  $t_w = 2.4\tau_\beta$  (e)  $f = 300$ ,  $t_w = 0.55\tau_\beta$  (f)  $f = 300$ ,  $t_w = 7.5\tau_\beta$

## 6.2 Transient Dynamical Response

Now we analyze in-plane single particle dynamics via evolution of self-vHfs between time  $t_w$  and  $t_w + t$ , given as  $G_S^{(+)}(r_{\perp}; t, t_w) (= \langle \sum_{i=1}^{N^{(+)}} \delta[r_{\perp}(t_w) + |R_{i\perp}^{\vec{}}(t_w + \Delta t) - R_{i\perp}^{\vec{}}(t_w)|] \rangle)$ . This quantity is averaged over the Brownian trajectories. We consider three typical values of  $t$  for three representative cases of  $t_w$  ( $t_w = 0, t_w \approx \frac{\tau_S}{2}$  and  $t_w \gg \tau_S$ ). We consider the cases  $f = 150$  (Fig. 6.2) and  $f = 300$  (Fig. 6.2) where the in-plane structural changes are significant. Let us consider the case for  $f = 150$ .  $G_S^{(+)}(r_{\perp}; t, t_w)$  is Gaussian in  $r_{\perp}$  for all  $t$  at  $t_w = 0$  [Fig. 6.2(a)]. For  $t_w \approx \tau_S/2$ , we observe that  $G_S^{(+)}(r_{\perp}; t, t_w)$  has an exponential tail around  $t = \tau_{\beta}$ . However, the tail disappears and  $G_S^{(+)}(r_{\perp}; t, t_w)$  reverts back to Gaussian at  $t = 10.5\tau_{\beta}$  [Fig. 6.2(b)].  $G_S^{(+)}(r_{\perp}; t, t_w)$  has exponential tail at  $t_w = 7.5\tau_{\beta} \geq \tau_S$  for  $t = 0.1\tau_{\beta}$ ,  $t = 4\tau_{\beta}$  and  $t = 6\tau_{\beta}$  [Fig. 6.2 (c)]. For  $f = 300$ ,  $G_S^{(+)}(r_{\perp}; t, t_w)$  is Gaussian at  $t_w = 0$  for all  $t$  [Fig. 6.3(a)]. At  $t_w \approx \frac{\tau_S}{2}$ ,  $G_S^{(+)}(r_{\perp}; t, t_w)$  is double-Gaussian in  $r_{\perp}$  at  $t (= 6\tau_{\beta})$  [Fig. 6.3(b)]. This double Gaussian behavior remains for all  $t$  in the steady state ( $t_w = 7.5\tau_{\beta} \gg \tau_S$ ) [Fig. 6.3(c)].

In order to quantify the behavior of  $G_S^{(+)}(r_{\perp}; t, t_w)$ , we fit  $\ln G_S^{(+)}(r_{\perp}; t, t_w) \sim -r_{\perp}^2/\sigma_{\perp}^2(t, t_w)$  for  $r_{\perp} < r_C(t, t_w)$  and  $\ln G_S^{(+)}(r_{\perp}; t, t_w) \sim a_T(t, t_w) - r_{\perp}/\lambda_{\perp}(t, t_w)$  for  $r_{\perp} \geq r_C(t, t_w)$  for  $f = 150$ . Similarly, for  $f = 300$   $\ln G_S^{(+)}(r_{\perp}; t, t_w) \sim -r_{\perp}^2/\sigma_{\perp(1)}^2(t, t_w)$  for  $r_{\perp} < r_C(t, t_w)$  and  $\ln G_S^{(+)}(r_{\perp}; t, t_w) \sim a_G(t, t_w) - r_{\perp}^2/\sigma_{\perp(2)}^2(t, t_w)$  for  $r_{\perp} \geq r_C(t, t_w)$ . We follow the fitting procedure as in Chapter 4.

We show  $a_T(t, t_w)$  and  $a_G(t, t_w)$  as function of  $t$  for different  $t_w$  in Figs.6.4(a) and (b) respectively. At  $t_w = 0$ ,  $a_T(t, t_w)$  show scattering [Inset Fig. 6.4(a)] where  $G_S^{(+)}(r_{\perp}; t, t_w)$  is a Gaussian. When the tail is insignificant,  $r_C(t, t_w)$  shifts to large values of  $r_{\perp}$ . In such cases, the fitting to the linear part becomes numerically unreliable and leads to large or small values of the amplitudes. Thus, scattered values in  $a_T(t, t_w)$  may be taken as indicative of absence of exponential tail. For small  $t_w \approx 0.1\tau_S$ ,  $a_T(t, t_w)$  decays with  $t$ . However, for  $t \approx 5\tau_{\beta}$ ,  $a_T(t, t_w)$  show scattering indicating insignificant tail. For  $t_w \approx 0.25\tau_S$ ,  $a_T(t, t_w)$  decays with  $t$  and gets scattered at  $t \approx 8.7\tau_{\beta}$ . Thus, the exponential tail becomes insignificant for large  $t$  for a given  $t_w$  although the tail stays longer with increasing  $t_w$ . We find  $\sigma_{\perp}(t, t_w)$  is linear in  $t$ . We examine  $\lambda_{\perp}(t, t_w)$  over time where the tail part of the self-vHf exists. In the steady states ( $t_w \gg \tau_S$ ), we observe  $\lambda_{\perp}^2(t, t_w) \sim t$  [main panel in Fig. 6.4(b)] indicating non-Fickian diffusion [44]. This is in agreement to our earlier result [23].

Similarly, for  $f = 300$ ,  $a_G(t, t_w)$  shows scattering at  $t_w = 0$  [Inset Fig. 6.4(c)] where  $G_S^{(+)}(r_{\perp}; t, t_w)$  is a single Gaussian. At  $t_w = 0.1\tau_S$ ,  $a_G(t, t_w)$  show scattering at  $t \approx 12\tau_{\beta}$  indicating that the second Gaussian becomes insignificant. However, for higher  $t_w$ , we do

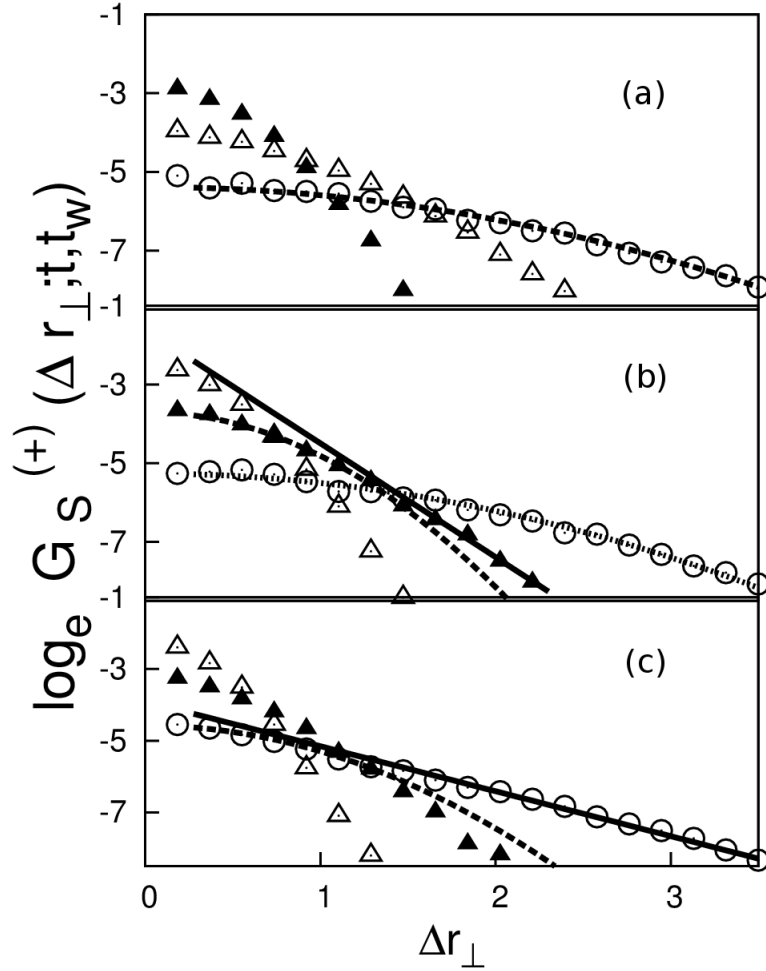


Figure 6.2:  $\ln G_S^{(+)}(r_{\perp}; t, t_w)$  as function of  $r_{\perp}$  for  $f = 150$  for  $t = 0.1\tau_{\beta}$  (open triangles),  $t = 4\tau_{\beta}$  (solid triangles) and  $t = 6\tau_{\beta}$  (open circles) at (a)  $t_w = 0$  (b)  $t_w = 1.2\tau_{\beta}$  (c)  $t_w = 7.5\tau_{\beta}$ . Dotted and solid lines show Gaussian and Exponential fits respectively.

not observe any scattering within our observation window. In all these cases,  $G_S^{(+)}(r_{\perp}; t, t_w)$  remains double Gaussian with two different widths (Inset. Fig. 6.4(c)). Thus, the double Gaussian nature persists for longer time with increasing  $t_w$ .

### 6.3 Aging in transient state:

We compute the mean squared displacements in the transverse plane,  $\langle r_{\perp}^2(t, t_w) \rangle (= \int r_{\perp}^2 G_S^{(+)}(r_{\perp}; t, t_w) dr_{\perp})$  for different  $t_w$ . We show the plots of  $\langle r_{\perp}^2(t, t_w) \rangle$  for two typical cases of  $t_w$  for both  $f = 150$  (main panel) and  $f = 300$  (inset) in Fig. 6.4(d). For  $f = 150$ ,  $\langle r_{\perp}^2(t, t_w) \rangle$  show changes in the slope with  $t$  for  $t_w = 0$ . For  $t_w \approx 3\tau_S$ ,  $\langle r_{\perp}^2(t, t_w) \rangle \sim t$ .

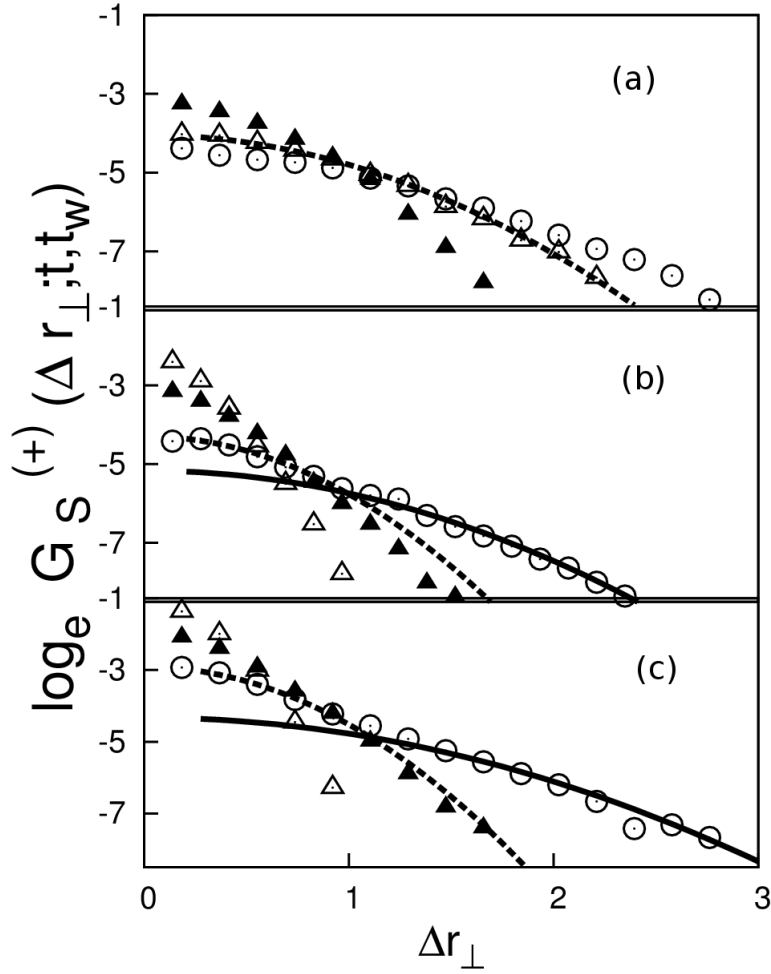


Figure 6.3:  $\ln G_S^{(+)}(r_{\perp}; t, t_w)$  as function of  $r_{\perp}$  for  $f = 300$  for  $t = 0.1\tau_{\beta}$  (open triangles),  $t = 4\tau_{\beta}$  (solid triangles) and  $t = 6\tau_{\beta}$  (open circles) at (a)  $t_w = 0$  (b)  $t_w = 1.2\tau_{\beta}$  and (c)  $t_w = 7.5\tau_{\beta}$ . Dotted and solid lines show two Gaussian fits with different widths respectively.

The data for  $f = 300$  are shown in the inset.  $\langle r_{\perp}^2(t, t_w) \rangle$  show different slopes with  $t$  then steadily increase with  $t$  for both  $t_w$ . However, for  $t_w \approx 3\tau_S$ ,  $\langle r_{\perp}^2(t, t_w) \rangle$  increase linearly with  $t$ .

The slopes of  $\langle r_{\perp}^2(t, t_w) \rangle$  gives diffusion,  $D(t, t_w)$  in between  $t_w$  and  $t_w + t$ . In Fig.6.5(a) we plot  $\frac{D(t, t_w)}{D_B}$  as a function of  $t$  for different  $t_w$  for  $f = 150$ . Here  $D_B$  stands for the self-diffusion coefficient in the equilibrium state. We observe  $D(t, t_w) \approx 3.5D_B$  for  $t \approx 0$  at  $t_w = 0$  and decreases to the steady value  $D_S \approx 1.2D_B$  for  $t \approx 2.0\tau_{\beta}$ . This time is comparable to  $\tau_S$ . At higher  $t_w$ , there is a decrease in  $D(t, t_w)$  at low  $t$  and decreases further with  $t_w$  and reaches  $D(t, t_w) \approx D_S$  at  $t_w \approx \tau_S$ . As  $t_w \sim \tau_S$ , the dependence of  $D(t, t_w)$  on  $t$  disappears and  $D(t, t_w) \approx D_S$  for all  $t$  in this case. The decrease in  $D(t, t_w)$  with  $t$  for a given  $t_w$  implies slowing down with time. The extent of slowing down depends on waiting time of observation

suggesting that the system shows aging which persists till it reaches structural steady state. As the system evolves from homogeneous liquid to the pre-lane state with larger domains of like charges with increasing  $t_w$  [Fig. 6.1], the system undergoes slowing down. This is reflected in statistical correlation between  $D(t, t_w)$  and  $\Delta\Phi$  [Inset, Fig. 4(a)]. We observe that  $D(t \approx 0, t_w)$  decrease with increase in  $\Delta\Phi$ .

Similar behavior has been observed for  $f = 300$ . At  $t_w = 0$  and  $t \approx 0$ ,  $D(t, t_w) \approx 5D_B$  which decrease rapidly with increasing  $t$  [Fig. 6.5(b)] and reaches steady value ( $D_S \approx 0.6D_B$ ) at  $t \approx \tau_S$ . For  $t_w = 0.25\tau_\beta$ ,  $D(t, t_w) \approx 3.5D_B$  for  $t \approx 0$  and the steady value is reached around the same timescale. For  $t_w \approx \tau_S$ , we observe  $D(t, t_w) \approx D_S$  for all  $t$ . Here also we observe that the signature of aging till the steady state is reached. We observe there is a decrease in  $D(t \approx 0, t_w)$  as the lanes appear in the system indicating increase in  $\Delta\Phi$  [Inset. Fig. 6.5(b)].

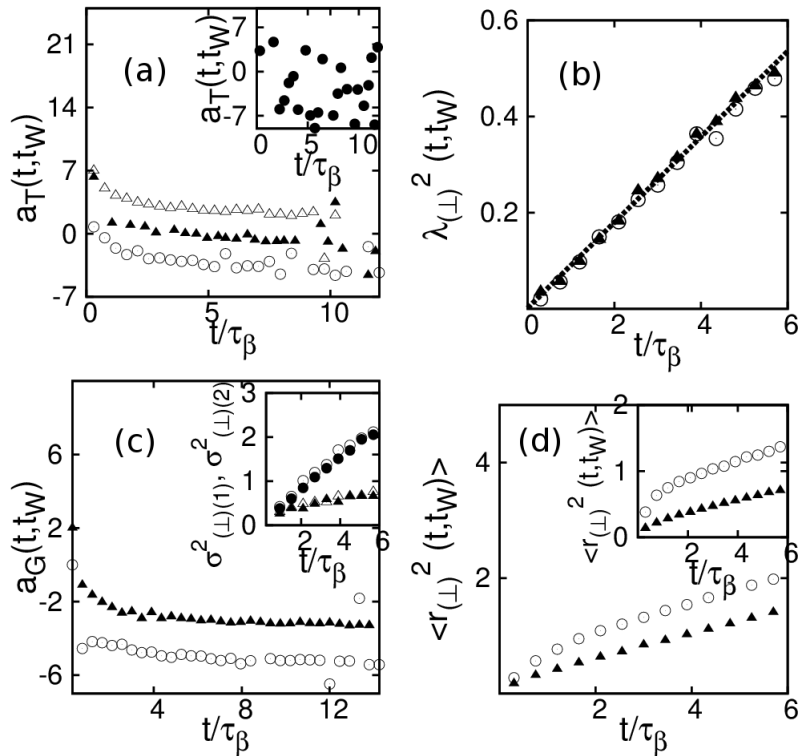


Figure 6.4: (a)  $a_T(t, t_w)$  as a function of  $t$  for  $\tau_S = 0.1\tau_S$  (open circles),  $\tau_S = 0.25\tau_S$  (filled triangles, with vertical offset 3),  $\tau_S = 2\tau_S$  (open triangles, with vertical offset 6) and  $\tau_S = 0$  (filled circles, in Inset) (b)  $\lambda_{(\perp)}^2(t, t_w)$  vs  $t$  for  $t_w = 2\tau_S$  (open circles) and  $t_w = 3\tau_S$  (filled triangles). (c)  $a_G(t, t_w)$  as a function of  $t$  for  $\tau_S = 0.1\tau_S$  (open circles),  $\tau_S = 0.25\tau_S$  (filled triangles, with vertical offset 3) Inset.  $\sigma_{(\perp)(1)}^2$  (circles) and  $\sigma_{(\perp)(2)}^2$  (triangles) as a function of  $t$  for  $t_w = \tau_s$  (open symbols) and  $t_w = 2\tau_s$  (filled symbols) (d)  $\langle r_{(\perp)}^2(t, t_w) \rangle$  vs  $t$  for  $f = 150$  (main panel) and  $f = 300$  (inset) for  $t_w = 0$  (open circles) and  $t_w = 3\tau_S$  (filled triangles).

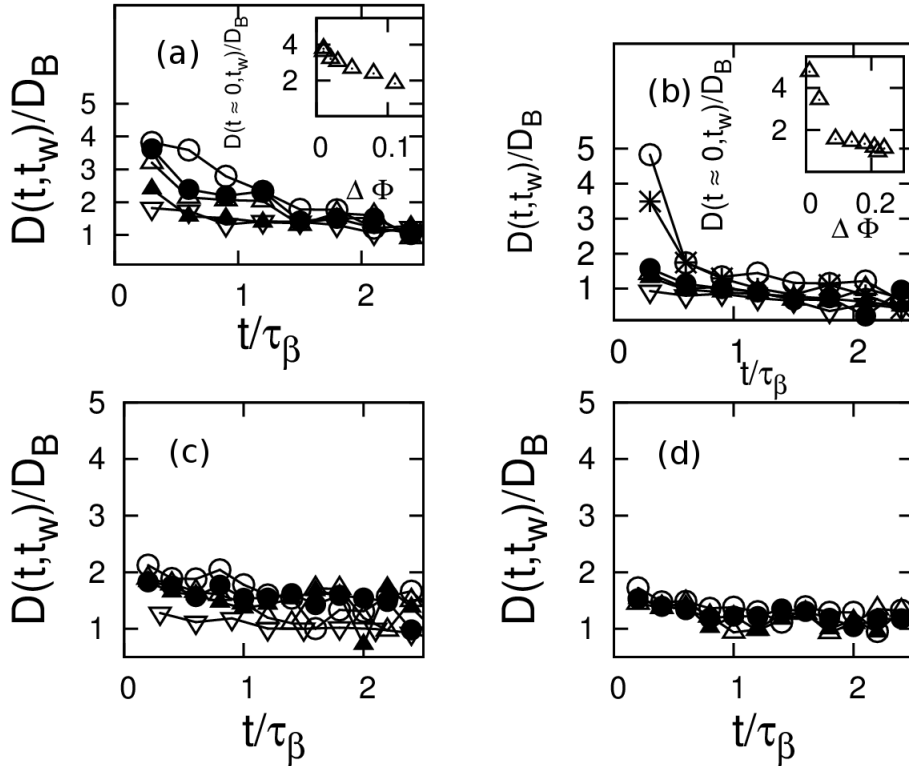


Figure 6.5: Dependence of  $D(t, t_w)/D_B$  on  $t$  for  $t_w = 0$  for (a)  $f = 150$  and (b)  $f = 300$  during growth of structure:  $t_w = 0.25\tau_\beta$  (filled circles),  $t_w = 0.5\tau_\beta$  (open triangles),  $t_w = 1.0\tau_\beta$  (filled triangles) and  $t_w = 1.5\tau_\beta$  (open inverted triangles). Insets. (a-b)  $D(t \approx 0, t_w)/D_B$  vs  $\Delta\Phi$  for (a)  $f = 150$  (b)  $f = 300$ .  $D(t, t_w)/D_B$  vs  $t$  for  $t_w = 0$  for (c)  $f = 150$  and (d)  $f = 300$  during relaxation of structure:  $t_w = 0.25\tau_\beta$  (filled circles),  $t_w = 0.5\tau_\beta$  (open triangles),  $t_w = 1.0\tau_\beta$  (filled triangles) and  $t_w = 1.5\tau_\beta$  (open inverted triangles). Lines are guide for the eyes.

## 6.4 Relaxation of Heterogeneous Structures

We also study the relaxation to equilibrium from the steady states at  $f = 150$  and  $f = 300$  by withdrawing the external field. Here  $\Delta\Phi$  approaches zero with increasing  $t_w$  with timescale  $\tau_S^R \approx 1.1\tau_\beta$  for the lane state and that around  $\tau_S^R \approx 1.3\tau_\beta$  from the pre-lane state (data not shown). As the states approach equilibrium,  $G_S^{(+)}(r_\perp; t, t_w)$  is Gaussian for all  $t_w$ , quite unlike the dynamical behavior during approach to non-equilibrium steady states in presence of field. We show  $D(t, t_w)$  for different values of  $t_w$  for  $f = 150$  in Fig. 6.5(c). For small  $t_w$ ,  $D(t, t_w) \approx 2.15D_B$  at  $t \approx 0$ .  $D(t, t_w)$  decreases with increasing  $t$  and saturates around  $D(t, t_w) \approx D_B$  at  $t$  close to  $2\tau_\beta$ . The dependence of  $D(t, t_w)$  on  $t_w$  is not significant in contrast to the growth case and does not show any  $t_w$  dependence in  $D(t, t_w)$  [Fig. 6.5 (d)]. In all the cases, the initial relaxation is fast followed by a slower relaxation in the vicinity of the

equilibrium state.

## 6.5 Discussion

We observe aging in lane forming binary colloids. Earlier, aging has been observed in super-cooled liquids [53] accompanied by slowing down in dynamics where the dynamical quantities depend on time of observation. The aging in our system is a transient phenomenon and lasts till the steady state is reached and connected to emergence of structural heterogeneity. The onset of structural heterogeneity is known as pattern formation [9]. Patterns are stabilized by competing inter-particle interaction as present in our system. Non-equilibrium patterns are relevant in variety of systems which are often described by coarse-grained models [9]. Microscopic calculations on pattern forming systems are not yet abundant: computer simulations on microscopic models have been performed on equilibrium patterns in binary mixture with competing interaction [61] and non-equilibrium pattern in glassy system under external perturbation [62]. There is a qualitative difference in the single particle dynamics of a glassy system and that of ours. In glassy systems the single particle dynamics is dominated by caging [53] due to neighboring particles. In contrast, the single particle dynamics in lane forming colloids is diffusive, albeit with heterogeneity in diffusion [23]. Such heterogeneous single particle dynamics is found in a variety of systems with complex interaction [44]. Our results are thus not only relevant in the context of lane formation but also would be pertinent in the emergence of patterns in soft matter systems with competing interaction under drive. This situation is often encountered in areas of rheology, micro-fluidics and bio-molecular systems [10].

The diffusion coefficients show slowing down in the transient conditions. The onset of heterogeneous structure shows aging in the transient state, while relaxation of structure proceeds without aging. Thus, the structural growth and relaxation takes place via different dynamical paths. This suggests inherent non-equilibrium nature of the transient responses.

## 6.6 Conclusion

We observe that the lane order parameter increases with  $t_w$  as the lanes grow in the system. The coarse grained particle distributions in the transverse plane shows growing domains with increasing  $t_w$ . We observe that the self-vHfs in the equilibrium state is Gaussian. As the system evolves, the self-vHfs develop exponential tail much before the steady pre-lane state sets in. Similarly, the self-vHf becomes double Gaussian before the laning is complete for larger field

strength. The time-dependent diffusion coefficients, are computed from the slopes of mean squared displacements, decreases with  $t_w$ . This behavior persists till the system attains steady state, suggesting aging in the system in the transient condition. When these steady state structures relax back to equilibrium upon withdrawal of the external electric field, the self-vHfs are Gaussian without any anomalous behavior. Our results could be verified by neutron scattering experiments on binary colloids and are expected to provide microscopic insights to pattern formation away from equilibrium.

# Chapter 7

## Dynamic Length-scales

The transient responses during the formation of lanes have been considered in chapter 6. In this chapter we consider the development of particle correlations during the formation of the lanes [28]. The particle correlations are described in terms of equal time density correlation functions (ETDCF). The ETDCFs in the transverse plane at time  $t_w$  is defined as  $g(\vec{r}, t_w) = (1/N^2) \langle \sum_{i=1}^N \sum_{j \neq i} \delta(\vec{r} + (\vec{R}_j(t_w) - \vec{R}_i(t_w))) \rangle$ . Here  $\langle \rangle$  implies averaged over the BD trajectories. We discuss the development in structural correlation in Sec. 7.1 and length-scales of correlation among different mobilities is discussed in section 7.2.

### 7.1 Length-scale of Structural Correlations

The equilibrated system for  $t_w = 0$  is shown via the particle snapshots in the XY plane, transverse to the applied field in Fig. 6.1(a). Here, no significant structure is observed. However, as soon as the field ( $f = 300$ ) is turned on, the structure undergoes changes. At small  $t_w (\approx 0.9\tau_\beta)$ , the tiny domains are observed [Fig. 6.1(e)]. The particles form network like patterns at  $t_w = 10\tau_\beta$  [Fig. 6.1(f)]. The structural changes in the transverse plane take place concurrently with the growth of the lane order parameter, defined in Sec. 2.3.2 in the system. The lane order parameter ( $\Phi$ ), defined in [17],  $\Delta\Phi(t_w) (= \Phi(t_w) - \Phi(0))$  reaches steady value ( $\approx 0.25$ ) at  $\tau_S \approx 1.2\tau_\beta$  [shown in Fig.6.1 (a)].  $\tau_S$  sets a natural timescale in the system.

Since both the charges behave similarly, we focus on the  $+ve$  charged particles. The ETDCFs between two  $+ve$  charges is given by  $g^{(++)}(r_\perp; t_w)$  and that between two opposite charges  $g^{(+-)}(r_\perp; t_w)$ . There is a peak in  $g^{(++)}(r_\perp; t_w)$  at  $r_\perp \approx 0$ , for all  $t_w$ . We denote this peak value by  $g^{(++)}(0)$ . The alignment into lanes in z-direction is quantified via  $g^{(++)}(0)$ . This quantity increases ( $g^{(++)}(0) \approx 8$  at  $t_w \approx 1.3\tau_\beta$ ) with increasing  $t_w$  and finally saturates, [Inset. Fig. 7.1(a)] indicating that the system has reached the lane state. We show  $g^{(++)}(r_\perp; t_w)$  for  $r_\perp \neq 0$

in Fig. 7.1(a) for different  $t_w$ . At  $t_w = 0$ ,  $g^{(++)}(r_\perp; t_w)$  no other peak for non-zero  $r_\perp$  is observed. With increasing  $t_w$ , ( $\approx 0.2\tau_\beta$ ),  $g^{(++)}(r_\perp; t_w)$  develops a tiny first coordination shell at  $r_\perp \approx 2\sigma$ . At  $t_w \approx 0.5\tau_\beta$ , the peak broadens and shifts to higher values in  $r_\perp$  and more peaks appear.

In contrast to  $g^{(++)}(r_\perp; t_w)$ ,  $g^{(+-)}(r_\perp; t_w)$  has a dip at  $r_\perp \approx 0$  and a peak at the first coordination shell at  $r_\perp \approx 1.1\sigma$  for  $t_w \approx 0$  [Fig. 7.1(b)]. At  $t_w \approx 0.3\tau_\beta$ , the peak shifts to  $r_\perp \approx 1.3\sigma$  indicating increasing population of opposite charges in the neighborhood of a lane. Like  $g^{(++)}(r_\perp; t_w)$ , in  $g^{(+-)}(r_\perp; t_w)$  more peaks are seen at higher  $r_\perp$  in for large  $t_w$  signifying increasing order between cross charges. The change in the dip at  $r_\perp \approx 0$  in  $g^{(+-)}(r_\perp; t_w)$  with  $t_w$  is probed via  $1 - g^{(+-)}(0; t_w)$  [Inset. Fig. 7.1(b)].  $1 - g^{(+-)}(0; t_w)$  increase and saturates with increasing  $t_w$  indicates the absence of opposite charges in a particular lane.

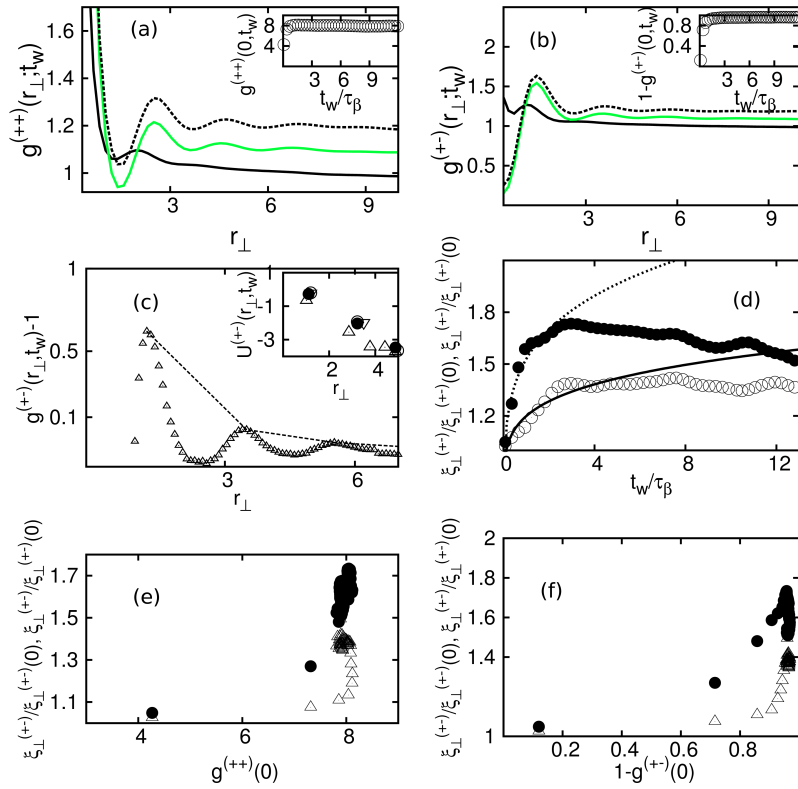


Figure 7.1: (a)  $g^{(++)}(r_{\perp}; t_w)$  vs  $r_{\perp}$  for  $t_w = 0.2$  (black solid line),  $t_w = 0.5$  (grey solid line, with vertical offset 0.1 unit) and  $t_w = 1.5$  (black dotted line, with vertical offset 0.2 unit) Inset.  $g^{(++)}(0; t_w)$  vs  $t_w$  (b)  $g^{(+-)}(r_{\perp}; t_w)$  vs  $r_{\perp}$  for  $t_w = 0.2$  (black solid line),  $t_w = 0.5$  (grey solid line, with vertical offset 0.1 unit) and  $t_w = 1.5$  (black dotted line, with vertical offset 0.2 unit). Inset.  $1 - g^{(+-)}(0; t_w)$  vs  $t_w$  (c) A typical example of  $U^{(+-)}(r_{\perp}; t_w)$  construction of  $g^{(+-)}(r_{\perp}; t_w) - 1$  as a function of  $r_{\perp}$ . Line show  $U^{(+-)}(r_{\perp}; t_w)$ .  $U^{(++)}(r_{\perp}; t_w)$  is constructed similarly (d)  $\xi_{\perp}^{(++)}$  (dotted line) and  $\xi_{\perp}^{(+-)}$  (solid line) as a function of  $t_w$ . Dotted and Dashed lines show  $\sim t_w^{0.2}$  dependence. (e)  $\xi_{\perp}^{(+-)}/\xi_{\perp}^{(+-)}(0)$  vs  $g^{(++)}(0)$  (filled circles),  $\xi_{\perp}^{(++)}/\xi_{\perp}^{(++)}(0)$  vs  $1 - g^{(+-)}(0)$  (open triangles), (f)  $\xi_{\perp}^{(++)}/\xi_{\perp}^{(++)}(0)$  vs  $g^{(++)}(0)$  (open triangles) and  $\xi_{\perp}^{(+-)}/\xi_{\perp}^{(+-)}(0)$  vs  $g^{(++)}(0)$  (filled circles)

To quantify the length-scale of the spatial correlation between the particles in the system, we first identify the local peaks in  $g^{(\pm\pm)}(r_{\perp}; t_w) - 1$ , for all  $t_w$  and construct an envelop  $U^{(\pm\pm)}(r_{\perp}; t_w)$ . A typical illustration is given in Fig. 7.1(c). For all  $t_w$ ,  $U^{(\pm\pm)}(r_{\perp}; t_w)$  decay exponentially with  $r_{\perp}$  [Inset. Fig. 7.1(c)]. We obtain the correlation length at time  $t_w$ ,  $\xi_{\perp}^{(\pm\pm)}(t_w)$  by fitting  $U(r_{\perp}; t_w) \sim \exp(-r_{\perp}/\xi_{\perp}(t_w))$  [65]. We observe  $\xi_{\perp}^{(++)}(0) \approx \xi_{\perp}^{(+-)}(0) \approx 1.0\sigma$  in the equilibrium system. In Fig. 7.1(d), we show the dependences of  $\xi_{\perp}^{(++)}$  and  $\xi_{\perp}^{(+-)}$  as a function of  $t_w$ . Both  $\xi_{\perp}^{(++)}$  and  $\xi_{\perp}^{(+-)}$  remains finite where  $\xi_{\perp}^{(++)} \approx 1.3$  and  $\xi_{\perp}^{(+-)} \approx 1.7$  at  $t_w \approx \tau_S$ .  $\xi_{\perp}^{(++)}$  fluctuates around a steady value  $1.4\xi_{\perp}^{(++)}(0)$  for large  $t_w$ .  $\xi_{\perp}^{(+-)}$  shows slight decay for large  $t_w > \tau_S$  so that there is a maximum around  $t_w \approx \tau_S$ . Both  $\xi_{\perp}^{(++)}$  and  $\xi_{\perp}^{(+-)}$  follow algebraic dependence ( $\sim t_w^{\alpha}$ ) with  $\alpha \approx 0.2$ .

We examine at the statistical correlation between the length-scales of particle correlations and the laning tendency in the system. We obtain this by eliminating  $t_w$  from both quantities [Figs. 7.2(e) and (f)]. Both  $\xi_{\perp}^{(++)}/\xi_{\perp}^{(++)}(0)$  and  $\xi_{\perp}^{(+-)}/\xi_{\perp}^{(+-)}(0)$  increases with  $g^{(++)}(0)$  initially but becomes uncorrelated for large  $g^{(++)}(0)$  [Fig. 7.1(e)]. Similar behavior is seen for  $1 - g^{(+-)}(0)$  [Fig. 7.1(f)]. This indicates that the correlations grow with laning tendency in the system. The structural correlations keep increasing even when laning order parameter remains unchanged. This is an indicative of coarsening. Similarly, the high values in  $\xi_{\perp}^{(+-)}$  and  $\xi_{\perp}^{(++)}$  appear in the steady states. In the steady states,  $1 - g^{(+-)}(0)$  has high value.

## 7.2 Dynamic Length-scales

In Chapter 4, we show that the particle diffusion spectrum has a peak at  $\approx 0.7D_B$  along with finite but small probability of high diffusion in the system. This indicates simultaneous presence of small and fast particles in the system. We tag the slow and fast particles in the system from particle displacement distribution between two configurations separated by time  $\delta t$  after  $t_w$ , given by  $P(\Delta r_{\perp}^2; \delta t, t_w)$ . We consider two configurations at time  $t_w$  and  $t_w + \delta t$  and compute the probability distribution of square of the particle displacements over different trajectories in the plane transverse plane,  $\Delta r_{\perp}^2$ . We fix  $\delta t (= 0.75\tau_{\beta})$ . The choice is made such that the changes in  $P(\Delta r_{\perp}^2; \delta t, t_w)$  are appreciable for all  $t_w$ . In Fig. 7.2(a), we show the evolution of  $P(\delta r_{\perp}^2; \delta t, t_w)$  as a function of  $\delta r_{\perp}^2$  for different  $t_w$ . For all  $t_w$ ,  $P(\delta r_{\perp}^2; \delta t, t_w)$  is asymmetric in  $\delta r_{\perp}^2$  with respect to the peak value. With increasing  $t_w$ , the peak in  $P(\delta r_{\perp}^2; \delta t, t_w)$  shifts to lower values of  $\delta r_{\perp}^2$ . We calculate the mean  $\mu(t_w)$  and standard deviation  $\sigma(t_w)$  of  $P^{(+)}(\Delta r_{\perp}^2; \delta t, t_w)$ . We show the dependence of  $\mu(t_w)$  [main panel in Fig. 7.2(b)] and  $\sigma(t_w)$  [Inset Fig. 7.2(b)] on  $t_w$ . With increasing  $t_w$ , both  $\mu(t_w)$  shifts to lower values with increasing  $t_w$  and saturates

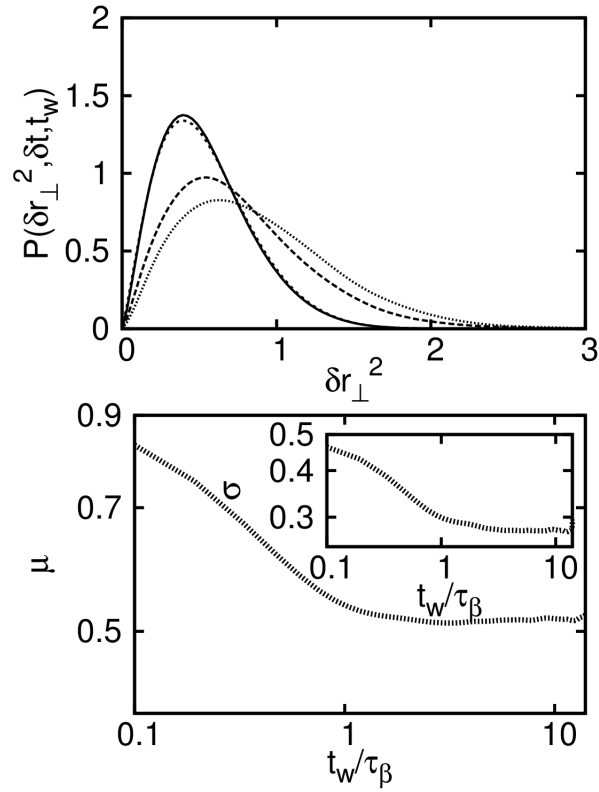


Figure 7.2: (a)  $P(\Delta r_{\perp}^2; \delta t, t_w)$  vs  $r_{\perp}^2$  for  $t_w = 0.3$  (grey dashed line),  $t_w = 0.5$  (black dashed line),  $t_w = 1.1$  (black dotted line) and  $t_w = 10$  (black solid line) (b) Dependences of  $\mu$  (main panel) and  $\sigma$  (inset) on  $t_w$

at  $t_w \approx \tau_S$ , indicating slowing down in the system. Similarly,  $\sigma(t_w)$  decrease with  $t_w$  and finally saturates beyond  $t_w \approx \tau_S$ . This indicates that mobilities get more homogeneous with increasing  $t_w$ . However, a finite heterogeneity persists in mobility in the lane state. In order to identify "slow" and "fast" particles at time  $t_w$ , we now tag particles of a particular species as "slow" (S) if it has displaced by  $\Delta r_{\perp}^2 < \mu(t_w) - \sigma(t_w)$ . Similarly, we tag the particles with  $\Delta r_{\perp}^2 \geq \mu(t_w) + \sigma(t_w)$  as "fast" (F). Thus we identify the  $N_S^{(\pm)}(t_w)$  no of "slow" particles of  $+ve$  and  $-ve$  charges respectively at time  $t_w + \delta t$ . Similarly, we count  $N_F^{(\pm)}(t_w)$  for the "fast" particles in the same time window.

We construct the ETDCFs of the 'fast' and 'slow' particles at  $t_w$ . The ETDCFs are given by  $g_{M,N}^{(++)}(t_w, r)$  where  $M$  and  $N$  stands for "fast" and "slow" particles respectively of the  $+ve$  particles. There are total six possibilities of the ETDCFs:  $g_{S,S}^{(++)}$ ,  $g_{F,S}^{(++)}$ ,  $g_{F,F}^{(++)}$ ,  $g_{S,S}^{(+-)}$ ,  $g_{F,S}^{(+-)}$  and  $g_{F,F}^{(+-)}$ . The envelopes of the correlation functions  $U_{(M,N)}(r_{\perp}, t_w)$  show exponential decay in  $r_{\perp}$  and are fitted by  $\exp(-r_{\perp}/\lambda_{(M,N)}^{(\pm\pm)}(t_w))$ . Here,  $\lambda_{(M,N)}^{(\pm\pm)}(t_w)$  are the spatial correlation length-scales of particles with different mobilities in the system. Both  $\lambda_{(S,S)}^{(++)}$  and  $\lambda_{(S,S)}^{(+-)}$  show increase with  $t_w$

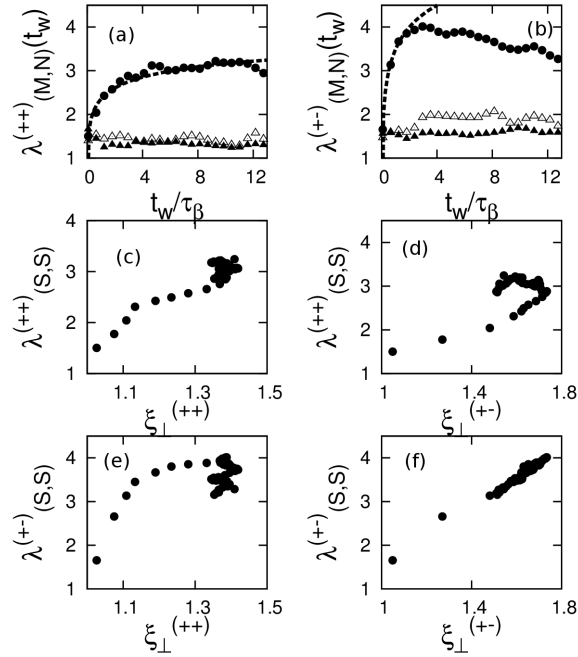


Figure 7.3: (a)  $\lambda_{(M,N)}^{(++)}(t_w)$  and (b)  $\lambda_{(M,N)}^{(+-)}(t_w)$  as a function of  $t_w$ ;  $M = S$  and  $N = S$  (filled circles),  $M = F$  and  $N = S$  (open triangles),  $M = F$  and  $N = F$  (filled triangles). dashed line show  $\sim t^\alpha$  dependence with  $\alpha \approx 0.2$ . (c)  $\lambda_{(S,S)}^{(++)}$  vs  $\xi_{(++)}$  (d)  $\lambda_{(S,S)}^{(++)}$  vs  $\xi_{(+-)}$  (e)  $\lambda_{(S,S)}^{(+-)}$  vs  $\xi_{(++)}$  (f)  $\lambda_{(S,S)}^{(+-)}$  vs  $\xi_{(+-)}$

for  $t_w \geq \tau_S$  [Fig. 7.3(a) and (b)]. These lengths become quite large, extending upto 3-4 particle diameter. We observe  $\lambda_{(S,S)}^{(++)}(t_w) \sim t_w^{0.16}$  and  $\lambda_{(S,S)}^{(+-)}(t_w) \sim t_w^{0.2}$  for  $t_w \leq \tau_S$ .  $\lambda_{(S,S)}^{(+-)}(t_w)$  decrease for  $t_w \gg \tau_S$ . This may be due to decreasing interface between two lanes of opposite charges with slow charges residing in the lane in presence of coarsening. The correlation lengths of the other species do not show significant change. Our data indicate that the correlation length between the slow particles in the system grow till the steady state is reached.

### 7.3 Discussion

We statistically correlate the data of mobility resolved correlation lengths,  $\lambda_{(M,N)}^{(\pm)}$  and the structural correlation lengths,  $\xi^{(++)}$  and  $\xi^{(+-)}$  in Figs. 7.3(c-f). We explicitly consider  $\lambda_{(S,S)}^{(++)}$  and  $\lambda_{(S,S)}^{(+-)}$  which show changes with  $t_w$ .  $\lambda_{(S,S)}^{(+-)}$  is linearly correlated to  $\xi^{(++)}$  with a difference in slope in the dependence around  $\xi^{(++)} \approx 1.1\xi^{(++)}(0)$ .  $\lambda_{(S,S)}^{(++)}$  becomes uncorrelated to  $\xi^{(++)}$  for large values  $\approx 1.3\xi^{(++)}(0)$  which corresponds to the steady states [Fig. 7.3(c)].  $\lambda_{(S,S)}^{(+-)}$  increase

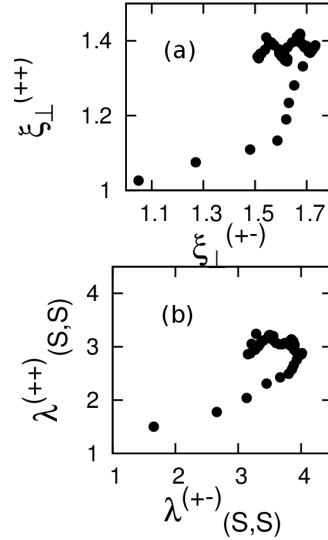


Figure 7.4: (a)  $\xi_{\perp}^{(++)}$  vs  $\xi_{\perp}^{(+-)}$  plot (b)  $\lambda_{(S,S)}^{(++)}$  vs  $\lambda_{(S,S)}^{(+-)}$  plot

for small  $\xi^{(++)}$ , but gets uncorrelated for large  $\xi^{(++)}$  [Fig. 7.3(d)] which corresponds to the steady states. We also correlate the two structural length-scales,  $\xi^{(++)}$  and  $\xi^{(+-)}$  in Fig.7.4 (a). For low  $\xi^{(+-)}$ ,  $\xi^{(++)}$  is correlated. For large  $\xi^{(+-)}$ ,  $\xi^{(++)}$  becomes uncorrelated. Similarly we correlate the dynamical length-scales,  $\lambda_{(S,S)}^{(++)}$  and  $\lambda_{(S,S)}^{(+-)}$ . They are correlated too for small values of  $\lambda_{(S,S)}^{(+-)}$  and become uncorrelated in steady states. These data indicates that there are four independent length-scales in the system in steady states.

## 7.4 Conclusion

To summarize, we show distinct behavior of correlation functions between different species. The structural correlation length between the like particles,  $\xi^{(++)}$  shows a  $t_w^{0.2}$  dependence upto  $t_w \sim \tau_S$  and thereafter it saturates.  $\xi^{(+-)}$  characterizing structural correlation between  $+ve$  and  $-ve$  particles varies as  $t_w^{0.2}$  within  $t_w \sim \tau_S$  but decays in the large time limit. The correlation lengths,  $\lambda_{(S,S)}^{(+-)}$  and  $\lambda_{(S,S)}^{(++)}$  behave similarly as  $\xi^{(+-)}$  and  $\xi^{(++)}$  respectively. In the steady states, these length-scales become independent.

# Epilogue

*I feel a very unusual sensation – if it is not indigestion, it must be gratitude.*

– Benjamin Disraeli

This thesis is a breed of my passion and emotions.

I am still in awe of my teacher at PHY205 (Spring 2010). It meant to be a regular course of computational physics. But Dr. J. Chakrabarti never touched the instructor-computer at AMRU-classroom for a single time in the whole semester. Yet it changed my vision, my goals, perhaps, the ways I used to think before. The course cooked something in me which I have never realized. I could only see me evolved.

Dr. Chakrabarti became Prof. Chakrabarti. Sharing science for more than six years with my advisor, Prof. Chakrabarti, is more than a privilege for me. There is always something I learn from each of the interactions with him, beyond the scientific wisdom. These build me stronger every day.

I cannot but forget the last class of PHY-105(Fall 2010). Prof. S. S. Manna gave me a ten rupee note (No-22C 259386, still kept at my bedside table) at the end of a marathon six hours class. My codes started running without bug after that. But I agree with Prof. Manna, Soumya (Soumyakanti Bose) was the most talented guy in our batch.

Soumya is the one whom I discuss every new things in life first. And definitely Pratik (Pratik Tarafdar). Together, we form CUBICLE ONE (Cubicle No. 1 at the Students Bay). We made possible every small impossible things: ScipiX (The very first SNBNCBS Magazine) to Muktangan (The first Cultural forum at SNBNCBS). There were also few good people around us: Victor (Dr. Victor U. J. Nwankwo), Arindam Da (Arindam Ghosh), I find your words reverberating around me.

I feel good when I look back to the life at GD-76 (2010-12). The time and the fun we had together, I would always cherish. Tejas (Tejas D. Rathod), I have retired from cricket after that match at the lawn. I have heartfelt gratitude for Arpan (Arpan K. Mitra) and Ankita (Ankita Chakrabarti) for the proxies on our behalf. Those nights right before the semester exams are

never going to come again.

How can I forget Dr. Debapriyo Syam? During 2009-10, while setting up the laboratory for upcoming M. Sc batch at the Barasat Government College, I had my first taste in research. Spending time with Prof. Syam at the lab, was more than joy. I still remember those rainy evenings when we walked together to Barasat station. I am lucky to have such moments of life.

There was Jyotish Kaku (Jyotish Chandra Roy). There was Kalyan da (Dr. Kalyanbrata Chatterjee). There were fights between three of us: me and two of my very first labmates, Parvez (A. M. Parvez Biswas) and Sabuj (Dr. Sabuj Ghosh) who used to compete every day to calibrate the spectrometer the fastest. There I had the finest company of Pallab (Pallob Paul), Debaleen (Debaleen Ghosh) and Santunu (Santunu Dey). There was Coffee House. There was college canteen. Indeed, there was life!

Life teaches a lot. Time proceeds from successes to mistakes. Mistakes show the path to success again. Success is an outburst of that agony. Agony comes from pain.

Pain comes from sacrifices:

To be a newly married husband towards the end of Ph. D is always difficult. Priyanka, I wish, someday, you would realize what it takes to ignore a lady like you, day after day, night after night. I wish, I would be a better husband some day.

Lastly but for-mostly, the two paraplegic kids at my home, Baba and Ma. I am lucky to have a father and mother like them. Words are not enough to express your sacrifice, the pain you're suffering currently, your efforts and supports.

This thesis is a tribute to everyone who contributed in shaping me.

# Bibliography

- [1] Nobel Lecture, P-G. de Gennes (1991).
- [2] S. R. Nagel, *Rev. Mod. Phys.* **89**, 025002 (2017)
- [3] R. A. L. Jones, *Soft Condensed Matter*, Oxford Master Series in Physics(Oxford University Press, Oxford, 2002)
- [4] D. David Andelman, and G. Reiter, (Ed) *Series in Soft Condensed Matter*, Vol-1-6, (World Scientific, Singapore, 2012).
- [5] H. Löwen, *Phys. Rep.* , **237**, 249 (1994); H. Löwen, *J. Phys. Condens. Matter* , **13**, R415(2001)
- [6] A. V. Blaaderen *et al.*, *Eur. Phys. J. Special Topics*, **222**, 2895 (2013); H. Löwen, *Eur. Phys. J. Special Topics*, **222**, 2727 (2013)
- [7] H. Löwen, *Soft Matter*, **6**, 3133 (2010)
- [8] D. Chandler, *Introduction to Modern Statistical Mechanics*, (Oxford University Press, 1987)
- [9] M. C. Cross and P. C. Hohenberg, *Rev. Mod. Phys.* **65**, 851 (1993)
- [10] I. S. Aranson, *Phys. -Usp.* , **56**, 79 (2013)
- [11] J. Dzubiella, G. P. Hoffmann and H. Löwen, *Phys. Rev. E*, **65**, 021402 (2002)
- [12] J. Chakrabarti, J. Dzubiella, H. Löwen, *Europhys. Lett.* , **61**, 415 (2003)
- [13] J. Chakrabarti, J. Dzubiella, and H. Löwen, *Phys. Rev. E*, **70**, 012401 (2004)
- [14] R. R. Netz, *Europhys. Lett.* , **63**, 616 (2003)
- [15] H. Löwen and J. Dzubiella, *Faraday Discuss.*, **123**, 99 (2003)
- [16] M. E. Leunissen *et al.*, *Nature*, **437**, 235 (2005)

- [17] M. Rex and H. Löwen, Phys. Rev. E, **75**, 051402 (2007)
- [18] K. R. Sütterlin, *et al.*, Phys. Rev. Lett., **102**, 085003 (2009)
- [19] T. Vissers, A. van Blaaderen, and A. Imhof, Phys. Rev. Lett., **106**, 228303 (2010)
- [20] T. Vissers, *et al.*, Soft Matter, **7**, 2352 (2011)
- [21] T. Glanz, and H. Löwen, J. Phys.: Condens. Matter , **24**, 464114 (2012)
- [22] M. Kohl *et al.*, J. Phys.: Condens. Matter, **24**, 464115 (2012)
- [23] S. Dutta and J. Chakrabarti, EPL(Europhys. Lett.), **116**, 38001(2016)
- [24] K. Klymko, P. L. Geissler and S. Whitelam, Phys. Rev. E, **94**, 022608 (2016)
- [25] A. Poncet *et al.* Phys. Rev. Lett. **118**, 118002 (2017)
- [26] S. Dutta, arXiv:1711.09779 (2017)
- [27] S. Dutta and J. Chakrabarti (pre-print)
- [28] S. Dutta and J. Chakrabarti (pre-print)
- [29] I. D. Couzin and N. R. Franks, Proc. R. Soc. London, Ser. B, **270**, 139 (2003)
- [30] D. Helbing, L. Buzna, A. Johansson and T. Werner, Transport. Sci., **39**, 1 (2005)
- [31] M. P. Ciamarra, A. Coniglio and M. Nicodemi, J. Phys.: Condens. Matter, **17**, S2549 (2005)
- [32] K. R. Sütterlin *et al.* , Phys. Rev. Lett., **102**, 085003 (2009)
- [33] F. Kogler and S. H. L. Klapp, EPL(Europhys. Lett.) , **110**, 10004 (2015)
- [34] P. Debye and E. Huckel, Physikalische Zeitschrift, **24**, 185 (1923)
- [35] B. Derjaguin and L. Landau, Physico Chemica URSS, **14**, 633 (1941)
- [36] E. J. W. Verway and J. Th. G. Overbeek, Theory of the stability of lyophobic colloids (Elsevier, Amsterdam, 1948)
- [37] D. L. Ermak, J. Chem. Phys. , **62**, 4189 (1975)
- [38] J-P. Hansen and I. R. McDonald, Theory of Simple Liquids (Academic Press, 2006)

- [39] L. van Hove, Phys. Rev. **95**, 249 (1954)
- [40] C. Dasgupta, A. V. Indrani, S. Ramaswamy and M. K. Phani, Europhys. Lett., **15**, 307 (1991)
- [41] S. Karmakar, S. Sastry and C. Dasgupta, Proc. Natl. Acad. Sci. USA, **106**, 3675 (2009), S. Karmakar, C. Dasgupta and S. Sastry, Annu. Rev. Condens. Matter. Phys **5**, 255 (2014)
- [42] M. P. Allen and D. J. Tildesley, Computer Simulation of Liquids (Oxford Science Publications, Oxford, 1989)
- [43] B. Smit and D. Frenkel, Understanding Molecular Simulation: From Algorithms to Applications (Academic Press, New York, 2002)
- [44] B. Wang *et al.*, Nat. Mat., **11**, 481 (2012).
- [45] T. Das, T. Lookman, and M. M. Bandi, arXiv:1505.05702 (2015)
- [46] J. D. Weeks, D. Chandler and H. C. Anderson, J. Chem. Phys. , **54**, 5237 (1971)
- [47] S. D. Stoddard, J. Comput. Phys. , **27**, 291, (1977)
- [48] A. J. Katz and A. H. Thompson, Phys. Rev. B. , **34**, 8179(R) (1986)
- [49] J. A. Greenwood, and M. M. Sandomire, J. Amer. Statist. Assoc **250**, 257-260 (1950)
- [50] G. H. Vineyard, Phys. Rev., **110**, 999 (1958)
- [51] S. Sengupta, and S. Karmakar, J. Chem. Phys., **140**, 224505 (2014)
- [52] S. Karmakar, C. Dasgupta and S. Sastry, Annu. Rev. Condens. Matter. Phys **5**, 255 (2014)
- [53] K. N. Pham *et al.*, Science, **296**, (2002), C. Donati, J. F. Douglas, W. Kob, S. J. Plimpton, P. H. Poole, and S. C. Glotzer, Phys. Rev. Lett. **80**, 2338 (1998)
- [54] E. E. Ferrero, K. Martens and J.-L. Barrat, Phys. Rev. Lett. , **113**, 248301 (2014);
- [55] Y. Guan, B. Wang, and S. Granick, *ACS Nano*, **8**, 3331-3336 (2014)
- [56] G. Kwon, B. J. Sung, and A. Yethiraj, J. Phys. Chem. B, **118**, 8128-8134 (2014)
- [57] K. Paeng *et al.*, Proc. Natl. Acad. Sci. USA , bf 112 4952(2015); R. Torre, P. Bartolini and R. Righini, Nature, **428**, 296 (2004); Pablo G. Debenedetti and Frank H. Stillinger, Nature, **410** 259 (2001)

- [58] L. Lucy, *B. Astron. J.* , **79**, 745 (1974)
- [59] S. Karmakar, C. Dasgupta, and S. Sastry, *Phys. Rev. Lett.*, **116**, 085701 (2016)
- [60] C. Donati, S. C. Glotzer, P. H. Poole, W. Kob and S. J. Plimpton, *Phys. Rev. E*, **60**, 3107 (1999)
- [61] R. Krishnan and S. Puri, *Phys. Rev. E* **92**, 052316 (2015)
- [62] G. P. Shrivastav, P. Chaudhuri and J. Horbach, *Phys. Rev. E*, **94**, 042605 (2016)
- [63] N. Cevheri and M. Yoda, *Lab Chip* **14**, 1391 (2014)
- [64] I. S. Aranson, *Phys. -Usp.* , **56**, 79 (2013)
- [65] J. Chakrabarti, *Phys. Rev. Lett.* ,**81**, 385 (1998)